Carbon-12 Reaction Rate on a Neutron Star in a Common Envelope Binary System

William Jack Jonathan Rudrum
Physics, Engineering and Technology
University of York
MSc by Research

August 2023

Abstract

In this thesis I calculate a new reaction rate for ^{12}C formed via the resonant reaction pathway that leads to formation of ^{12}C in an excited state known as the Hoyle State. This research was precipitated by the discovery that the radiative width (Γ_{rad}) was 34 percent higher than the previously accepted value[1]. This is considerably larger than the uncertainty on the previously accepted value. I then used a scaling factor to assess the impact a higher rate could have on nucleosynthesis models using NuGrid. The astrophysical environment simulated was for a neutron star in a common envelope binary system. The neutron star spirals towards the centre of a late stage red giant; which provides the helium rich environment and the extreme temperature and pressure that is perfect for explosive nucleosynthesis to occur. A primary example of explosive nucleosynthesis is the triple alpha process investigated by this research. My results, having used a scaling factor that increased the triple alpha reaction rate by 30 percent in line with my results. This appears to cause a significant increase in the abundance of ^{12}C, in some instances 3 times more ^{12}C is present compared to simulations using the old reaction rate. This is the first time this has been investigated in this astrophysical environment. My results clearly show that Nucleosynthesis models are significantly impacted by the higher reaction rate for Carbon-12.

Contents

List of Figures

1 Acknowledgments

I would like to thank the members of the NuGrid Collaboration, both current and former, without whom the tools I used to conduct my simulations, would not be available. I'd like to thank Alexander Hall-Smith and Sophie Abrahams for answering all my questions and helping me to debug code and Sophie for providing some python code that was helpful in analysing my outputs. I would also like to thank my Supervisors Dr Christian Diget and Dr Alison Laird. Without their guidance and teaching I would not have been able to complete this. Finally, I'd like to thank my family who encouraged and supported me throughout.

2 Declaration

I declare that this thesis is a presentation of original work and I am the sole author. This work has not previously been presented for an award at this, or any other, University. All sources are acknowledged as References.

3 Introduction

This project is on the nucleosynthesis of carbon-12 on a Neutron star in a common envelope binary system. Carbon-12 and the rate at which it forms through nucleosynthesis in stellar environments is important for a few reasons, two examples of which are that it effects the rate of formation of heavier elements and thus their abundance and also because carbon is crucial for life to exist [12]. This project examines the reaction rate for Carbon-12 formation via the resonant reaction pathway that leads to stable carbon-12 formation, via what is known as the Hoyle State [13]. The resonant reaction rate is being re-examined in this project due to a recent development outlined in the paper "Radiative Width of the Hoyle State from Gamma-Ray Spectroscopy". The paper concluded that "the radiative width of the Hoyle state is determined as Γ_{rad}=5.1(6)x10^{-3} eV. This value is about 34 percent higher than the currently adopted value"[1] and as such could have noticeable effects on stellar nucleosynthesis models. This is the main motivation behind the work undertaken as part of this project. The aim is to establish if the new reaction rate that results from the new Γ_{rad} for Carbon-12 formation via the Hoyle state has a noticeable effect on the output of stellar nucleosynthesis using NuGrid.

3.1 MSc Thesis Outline

The thesis will be separated into multiple sections/chapters. This first section is the introduction to the project which includes the details of my motivation for undertaking this research and what it hopes to achieve. Section 2 will cover the background, theory beginning with the theory behind the astrophysical stellar environment of the scenario, that is being used to investigate the potential impacts upon the stellar nucleosynthesis model. Section 3 will then follow on with the nuclear theory behind Nucleosynthesis. Section 4 will cover the methodology for how I carried out my work. This will include calculating a new reaction rate for Carbon-12 formation via the Hoyle state. I will then detail how it was implemented into NuGrid. Section 5 will deal with presenting the data from my work and analysing it before section 6 summarises my analysis and the conclusions I will draw from that and suggest ways in which the work could be built upon in the future. In addition; I will discuss the limitations of the project.

4 Stellar Environments

The stellar environment is important because it determines the specifics of the physical processes that you would expect to be occurring. From fission to fusion and nucleosynthesis of elements in stars, to the crushing and spagettification of matter on its approach to a black hole, the subsequent compacting of matter to densities that warp space-time beyond recognition, or to neutron stars so dense that a single teaspoon of their exotic matter [14] would likely have a mass similar to that of the whole earth. All of these are examples but by no means an exhaustive list of the extreme environments that can be found in the universe and are excellent settings to observe and model various aspects of physics theory to test them to their limits. In some cases they are the only locations where the conditions exist for the processes to occur naturally. Therefore, the specific astrophysical environment that is the site for the physics being studied is very important, as it will underpin all of the specific conditions (temperature, density, abundance of various particles etc) and how those conditions evolve over time for any modelling being done.This extends to both the macroscopic and microscopic level.

4.1 Binary Stars

Firstly, binary stars should not be mistaken for ”double stars”; double stars are simply stars that appear to be near each other in space but they are not. Historically what we now refer to as Binary stars were sometimes referred to as double stars. The modern definition of a binary star is generally defined as two stars which orbit a common centre of mass[15]. The two stars are by convention referred to as the primary and the secondary star; the primary star is the one with the higher brightness of the two.

These systems have two classifications, close binaries and far binaries. A far binary has a large orbital path and the stars whilst orbiting the same centre of mass largely don't interact with one another and evolve independently. The second classification is Close Binaries. They are much closer to one another and as such their evolution is intrinsically tied to that of the partner star; they can often share mass from one star to another as is the case in a common envelope system. These stars fall into a number of sub categories. These are:

- Visual Binaries: a visual binary is a binary star system where the orbit of the stars can be observed through observation via a telescope alone due to quite wide orbits.
- Spectroscopic Binaries: these stars have very close orbits and even through a telescope cannot be distinguished from a bright ordinary star. Instead the binary must be discovered through analysis of the light they emit using spectroscopy.[15]
- Eclipsing Binaries: as their name suggests they orbit with an orbit that results in one star passing in front of the other and 'eclipsing' it from view, at least as per the perspective of earth[16].
- Astrometric Binaries: in the case of an astrometric binary only one of the stars can be observed the other's existence is simply inferred through the behaviour of the primary star which will appear to be orbiting empty space [17].

In addition to these different categories you can also factor in the different types of stars and the combinations that can occur and the various outcomes of those combinations. For example two close binary neutron stars are likely to result in a neutron star merger. This can lead to either a larger neutron star being created or potentially a black hole [18]. A neutron star-neutron star binary is created when two large stars, possibly in a binary system end their lives through an explosive supernova leaving behind two neutron stars. Further examples would be a close binary [19] where the primary star becomes a red giant or simply progresses to the later stages of a red giant's life cycle, whilst it is part of a binary star system with a neutron star as the secondary star. Due to the close nature of the stars it is likely they would be a spectroscopic binary and would have formed what is known as a common envelope. This specific example is the astrophysical scenario that formed the backdrop for my research into the reaction rate of carbon-12 during nucleosynthesis on a neutron star in a common envelope binary.

4.2 Red Giants

Over their lifetime stars change considerably. Where they are in their life-cycle and their temperature, size and various other properties, ares determined by what elements they are now fusing together. Heavier elements are formed through fusion in the latter stages of a star's life when lighter elements have been depleted. A red giant begins as a main sequence star with a mass of approximately 0.5-5 solar masses[20] (the majority of stars in the observable universe fall into this category).The Hertzsprung-russell diagram in figure 1 shows the different stages of a stars life and the different classes stars fall into.

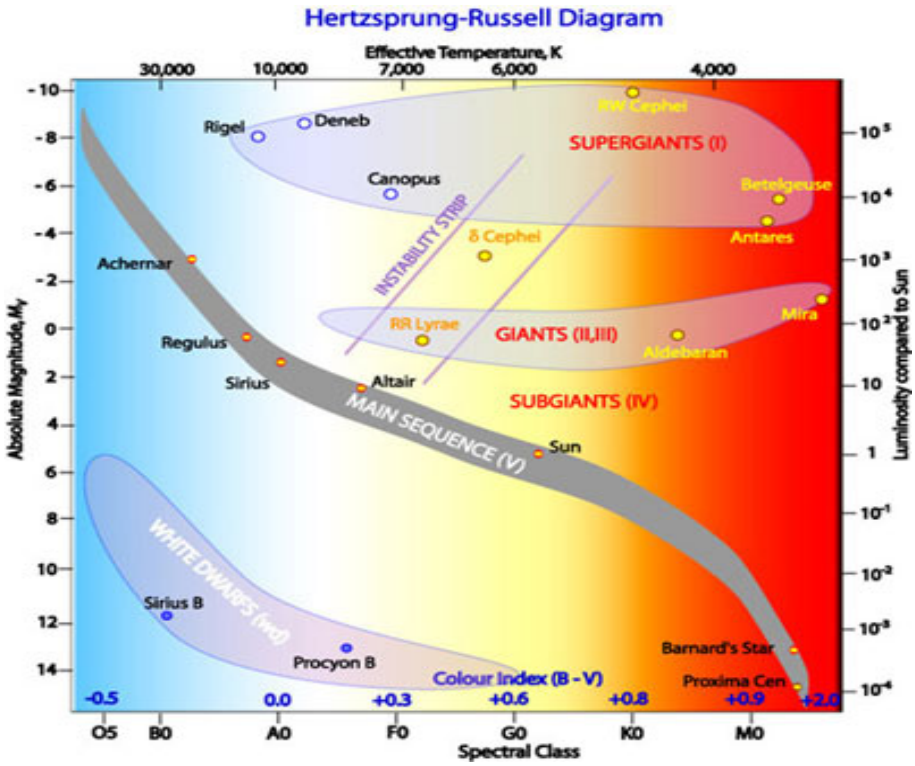

Figure 1: A Hertzsprung-russell Diagram showing the different types of star and some of their properties.[2]

A main sequence star is a star in the primary sequence of it's life-cycle; this is the part of it's life that occurs after it's initial formation and it will be primarily fusing hydrogen to form helium and it's outer layers will be hydrogen rich. The fusion process generates outward pressure which balances the inward pressure caused by the gravitational pull of the material that the star is formed from. However, as this causes outward radiation pressure from this shell to increase, this causes the outer layers of the star to expand. The effective temperature of the star decreases due to it's expanded size and typically will now be about 3000 Kelvin [11]. The star is now a red giant. Red giants vary in size considerably and can be between 100 million kilometers to 1 billion kilometers in diameter [12].

4.3 Neutron Stars

A neutron star is a star late in it's life-cycle that is made entirely of neutrons. It is incredibly dense with a single teaspoon of it's neutron dense material having the equivalent mass of approximately 4 billion tonnes[13]. They vary in size but on average measure about 12km across in radius[21]. Neutron stars come in a few different forms, most of the neutron stars that we have observed fall into the category of being a pulsar[14]. A pulsar is a spinning neutron star with a strong magnetic field. As it spins, charged particles present on it's exterior are lifted up from the surface and slammed back down at the opposite magnetic pole;this process creates a large pulse of electromagnetic radiation, which we can detect on earth. Pulsars can emit a range of electromagnetic

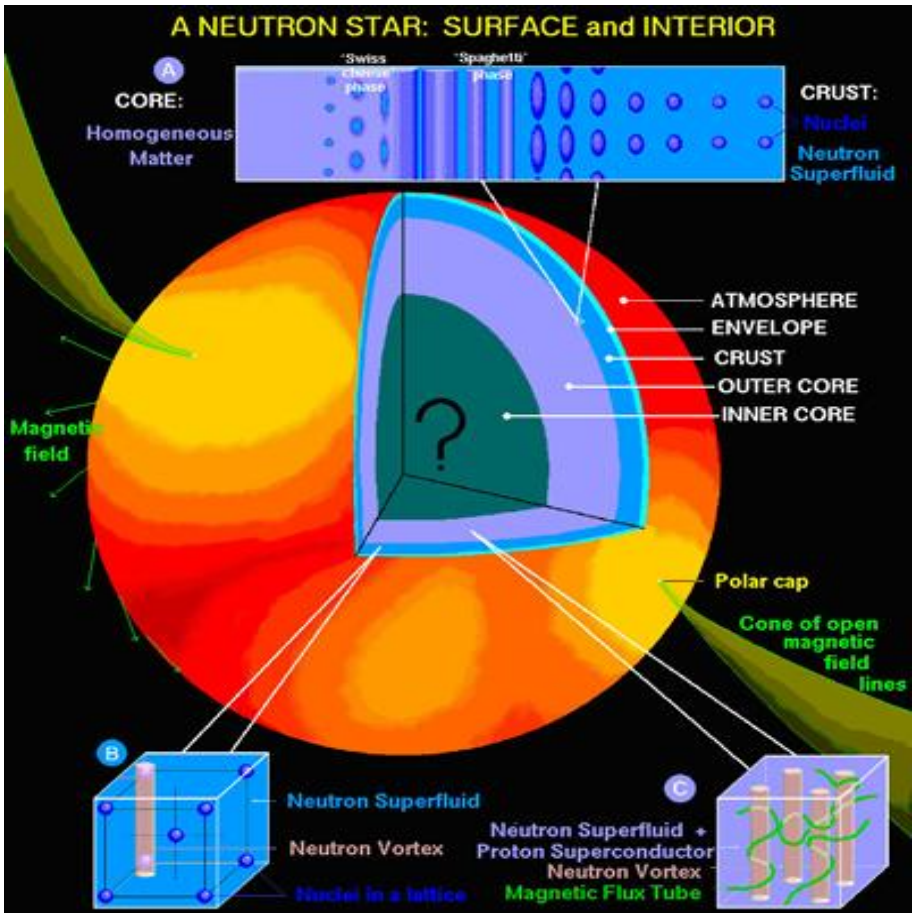

Figure 2: Shows the theoretical makeup of a neutron star. [3]

radiation and have sub categories dependant upon the type of radiation they emit; examples of the emissions are radio waves, x-rays and gamma-rays. The radiation emitted is linked to how fast the stars are rotating with faster rotating neutron stars emitting shorter wavelength electromagnetic radiation. Magnetars are another form of neutron star, they are characterised by their incredibly strong magnetic fields which are in the region of 10^9 to 10^{11} Tesla [22]. Some of the magnetars are known as "Soft Gamma Repeaters"[23] as they emit gamma-radiation in busts that seemingly occur at random. Magnetars are quite rare and at present we have only identified 31[24] of them in the known universe.

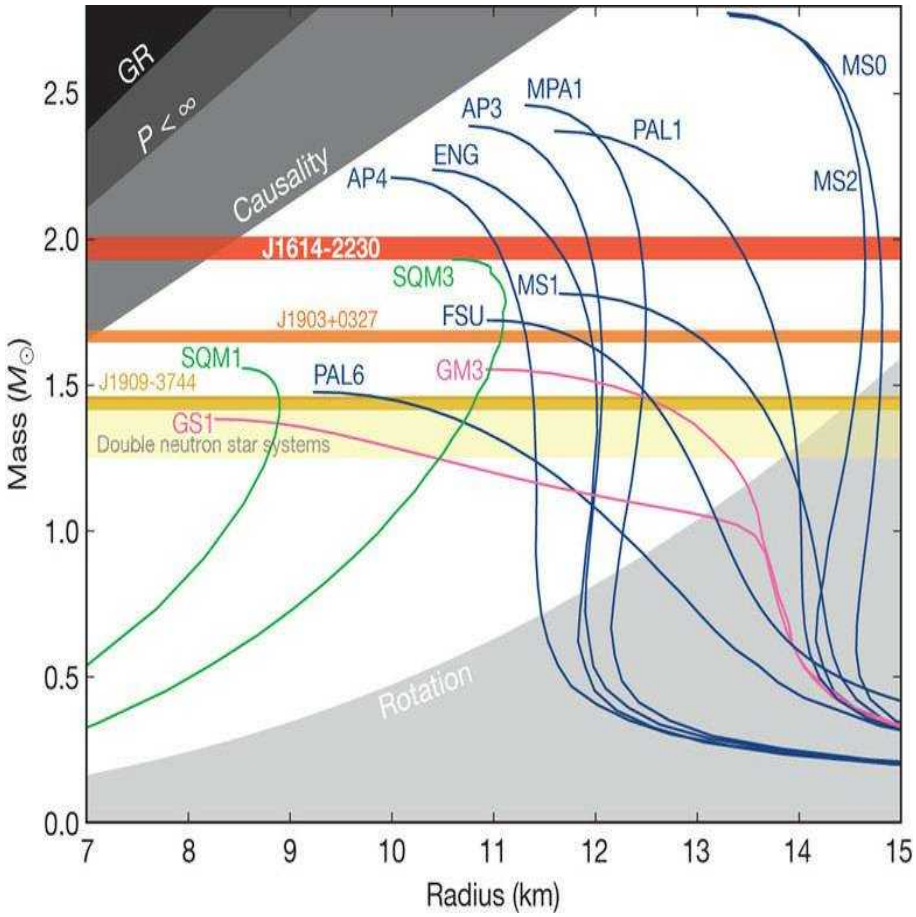

Figure 3: A graph showing potential neutron mass/radius curves for different models of potential neutron star particle makeup. Nucleonic is blue, Nucleonic plus exotic particles is pink and strange quark matter models are green.
[25].

The graph in figure 3 shows mass-radius curves for various models of Neutron stars depending upon their makeup. As you can also see in the graph there is an orange band labelled after the Neutron star it represents. Star J1614-2230 which has a mass similar to that of the of the mass I chose for my simulations(2.0 solar mass). At roughly 1.9 Solar Masses [26] according to the most recent measurements, the importance of J1614-2230 cannot be understated. J1614-2230 existence demonstrates that the relevant properties chosen for my simulations do represent a realistic astrophysical scenario and also seem to indicate potential limitations on the models for the internal composition of neutron stars as-well. It suggests that a neutron star with a mass of 2 solar masses would have a radius between approximately 11km and 14.8km.

4.4 Common Envelopes

A common envelope binary is what would be classified as a spectroscopic close binary system, a system that contains a red giant or other gas star as the primary star and a neutron star as the secondary. Due to their closeness their orbits may not be stable in

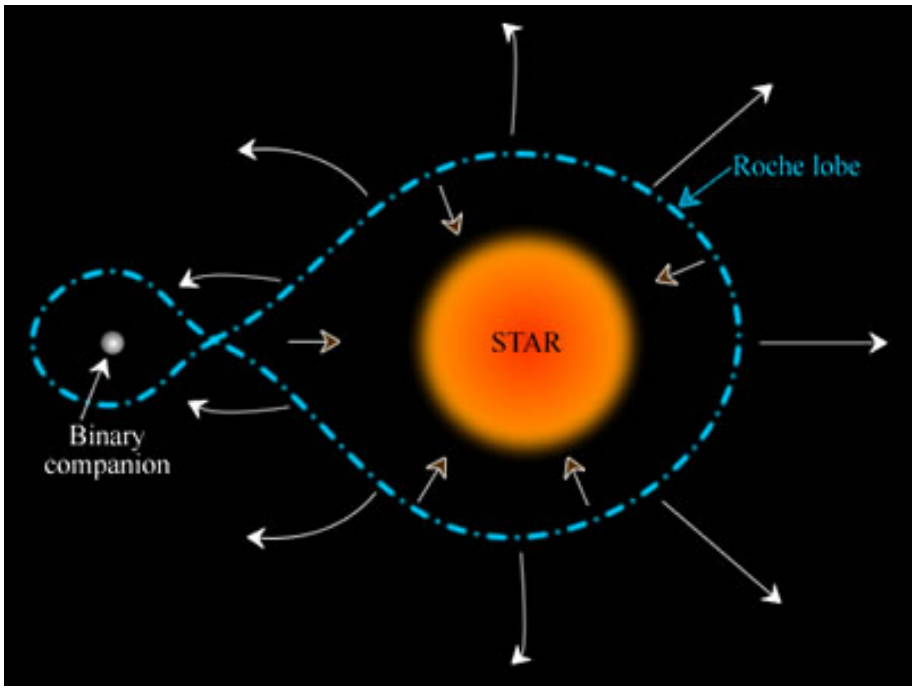

Figure 4: Figure 4 shows a diagram of a roche lobe prior to accretion occurring [4].

which case they would slowly move closer together until the neutron star is engulfed in the outer edges of the primary star. There are other ways this can happen however; such as when a red giant is formed or progresses in it's life-cycle and expands, engulfing the neutron star. (I feel it important to state that the secondary star doesn't have to be a neutron star; it can be another type of star. The same general concept applies). When the secondary star is engulfed by the primary star's outer gas shells, frictional forces will impact on the orbit. The secondary star will spiral towards the primary star. Whilst this happens the orbiting star accretes material from the larger star. This can occur at various different rates and the rate at which this material accretes has an effect on the temperatures and densities within the material and thus the rate at which fusion occurs. For the purposes of my work- the scenario I examined was a neutron star orbiting a late stage Red Giant. The area in which the material it's accreting is bound to either star, is known as the Roche lobe. The Roche lobe is essentially a figure of 8 around each star with the centre of each part of the 8 being the primary and secondary star. It describes the influence of gravity over material orbiting or passing by the stars. The area of the 8 around the secondary star fills with material from the primary star. If the accreting material is of sufficient volume that it expands beyond the confines of the figure of 8, it can fall back towards the primary star and will then be under the primary influence of it's gravitational forces. Figures 4 and 5 show a diagram of Roche lobe and the transfer of mass between the primary and secondary star.

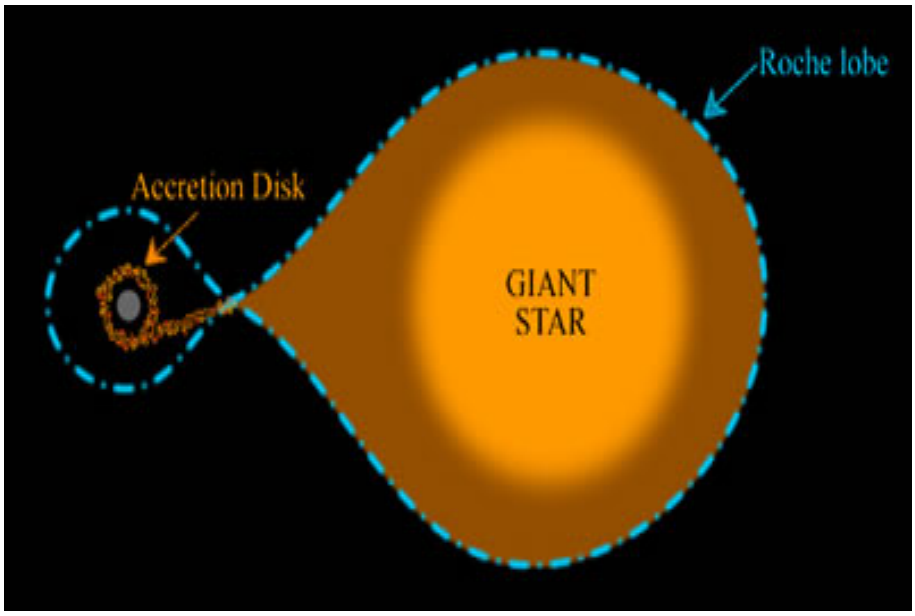

Figure 5: An example of the Roche lobe as accretion occurs, shows the accretion disc around the secondary star[5].

4.5 Accretion Rates

Accretion in the astrophysical use of the term refers to the gradual acquisition of matter by an object due to gravity [27]. It occurs in a wide variety of scenarios, from the formation of stars which start as a gas cloud which gradually clumps together to the formation of planets from initially small clumps of metal or rocky material. Due to the way gravity pulls mass towards the centre of mass of an object with equal strength from all directions, this naturally leads to mass that accretes forming a spherical shape for an individual object. In the common envelope binary scenario as shown in figure 4 and figure 5, the shape is more likely to be oval due to the influence of the donor star's gravity. This can be seen in figure 4 and 5 the diagram of a Roche lobe. The accretion rate is particularly important for a common envelope scenario involving a neutron star because of the relationship between the mass of the object that is accreting material. This has a direct impact on the energy the particles have, the temperatures reached and therefore the extreme conditions that can be found on a neutron star in a common envelope; and that has implications for the types of nucleosynthesis that can occur here, specifically the formation of heavier elements which require extreme temperatures and pressures that are not common occurrences in the universe.

$$\Delta E_{acc} = \frac{GM_{NS}m}{R_{NS}} \tag{1}$$

Where R_{NS} is the radius of the Neutron star. Formula 1 [28] shows the energy generated from the infall of matter towards the surface of a Neutron star. The process is, due to the incredibly dense nature of a neutron star, considered incredibly efficient. This high energy is what helps to create the extreme conditions previously mentioned that can be found in a common envelope scenario.

4.5.1 Eddington Luminosity

As the accretor accrues material, it's temperature increases as does it's density near the centre (or in the case of my model; the surface of the Neutron star). After a certain point this will mean that frictional forces and nuclear reactions are going to be causing energy to be emitted by the accretion disc and as a result of that radiation will be emitted. The ionising radiation collides with other particles and is a source of energy moving outwards, creating an outward radiation pressure. It is entirely possible for an equilibrium point to be met where the gravitational forces are balanced by the outwards pressure caused by the radiation. The Luminosity at this point can be described by equating the radiation pressure to the gravitational potential [29]:

$$\frac{GmM}{R^2} = \frac{Lkm}{4\pi R^2 c} \tag{2}$$

$$k = \sigma_T / m_p \tag{3}$$

so:

$$L_{Edd} = \frac{4\pi GMcm_p}{\sigma_T} \tag{4}$$

Where G is the gravitational constant, M is the mass of the central object,of the primary and secondary stars, R is the radius, L is the , C is the speed of light m_p is the mass of a proton and sigma T is the Thompson cross-section.

4.5.2 Eddington Limit

So,the rate at which the material accretes as well as the mass of each body and (thus the acceleration of accreted material towards the centre of the larger body) determine the luminosity. Now the Eddington luminosity describes the luminescence of the equilibrium point.Therefore, it also determines the radiation pressure from the core pushing outwards. The Eddington limit as described in equation 5, expands on this concept and describes a situation where the outwards pressure from radiation exceeds that of the inwards force from gravity and results in large amounts of the material that has accreted being blown off into space. This is the result of the accretion rate becoming too high for the mass of the object that the material is accreting around. This is one potential way that heavier elements formed through nucleosynthesis within a common envelope scenario, exit the envelope and are spread around the universe and then go on to be part of the formation of planets for example.

$$M_{EDD} = \frac{4\pi GMm_p}{\varepsilon c \sigma_T} \tag{5}$$

Equation 5 shows the equation for the Eddington limit. Epsilon is the radiative efficiency.

5 Stellar Nucleosynthesis

Stellar nucleosynthesis is the formation of different elements and their various isotopes through nuclear reactions in a variety of different stellar environments. Lighter elements release energy when they fuse; however, as they get heavier the energy released from fusion decreases until eventually they use more energy (This will be discussed in greater detail later in this chapter). Stars later in their life-cycle as such have a higher abundance of heavier elements and their formation contributes to a star's death. This could well be a simple environment like an individual star like the sun or a more complex environment like a supernova, or two stars in a binary system in a common envelope.

5.1 Nuclear Theory and context within Astrophysical setting

Historically, it was hard to measure the mass of a nucleus with all the electrons stripped away, as such the atomic mass (M_n) is determined using the relationship:

$$M_a = M_n + Zm_e - B_e(Z)/c^2 \tag{6}$$

m_e is the rest mass of an electron ($9.109x10^{-31}kg$ or 0.511 MeV/c^2) [30] and the value $-B_e(Z)/c^2$ is the binding energy of the electrons.

Ultimately, this leads to the total mass of the nucleus of an atom being less than the mass of its constituent parts. This difference is known as the nuclear mass defect and can be written as [31]: $\Delta M_n = M_n - ZM_p - NM_N$ and represents an energy difference of $\Delta E = \Delta M_n c^2$. This is the energy released in assembling the nucleus from it's constituent nucleons and is acquired at the cost of the mass of the nucleus, it is also the energy required to separate the different parts of the nucleus and in that context is referred to as the binding energy.

The binding energy is why nuclear fusion of lighter elements releases energy and fission of heavier elements does the same. The graph in figure 3 shows the binding energy per nucleon in atomic nuclei plotted against the mass number.

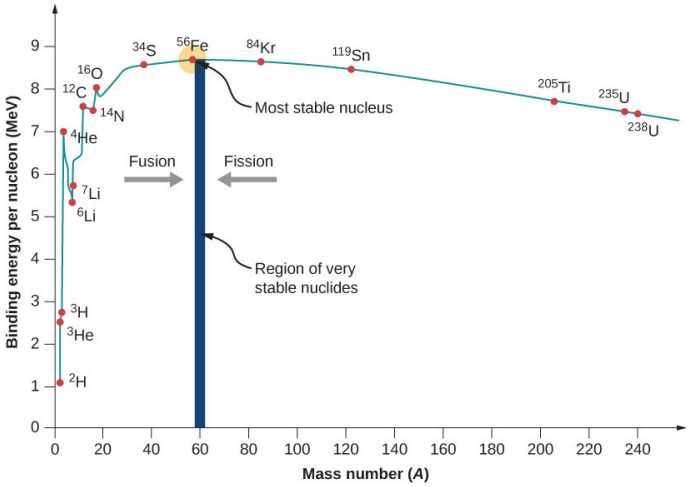

Figure 6: The binding energy per nucleon plotted against the mass number of the element[23].

Elements smaller than Iron; which has 26 protons and an average mass of 55.8 AU [32] and as can be seen in figure 6 has the most tightly bound nucleus- release energy when fused together.

Nucleosynthesis is the process whereby nuclear fusion occurs to form new elements. Fusion occurs when protons or the nuclei of atoms are able to overcome the coulomb barrier and thus fuse to form new heavier elements. Sometimes this process can also involve the formation of unstable isotopes and subsequent nuclear decay to a more stable isotope of the same or another element as an additional part of the process. Due to the relationship shown in figure 6 between the binding energy and the mass of isotopes, the process eventually begins to use up more energy than it produces, which is what leads to a star's death and places limits on when heavier elements can form. The fact that energy is required, not released and that the Coulomb barrier's value increases as the atomic nuclei involved in the process get larger (due to the increased number of protons) means heavier elements require considerably more energetic environments to be formed such as, for example, a supernova.

5.2 Reaction Rates

Nuclear reactions are typically written in the format:

$$a + X \rightarrow Y + b \tag{7}$$

Where X and Y are Nuclei and a and b are other particles that are part of the process being described.

For example if we take the decay of Radon gas which is notorious for decaying via alpha decay it would look like [33]:

$$^{226}_{88}Ra \rightarrow ^{222}_{86}Rn + ^{4}_{2}He \tag{8}$$

whilst for a simple fusion reaction of deuterium the equation would look like [34]:

$$^{2}_{1}H + ^{2}_{1}H \rightarrow ^{3}_{2}He + ^{1}_{0}n + 3.27MeV \tag{9}$$

The $^{1}_{0}$n in equation 9 represents a neutron and in this instance the excess energy released from the reaction is also listed, although this is likely emitted in the form of electromagnetic radiation otherwise known as a photon.

If you were to imagine the two particles in the hydrogen fusion example above as being like a pair of marbles, then the classical description of the cross section would be as follows:

$$\sigma = \pi(r_1 + r_2)^2 \tag{10}$$

Equation 5 is basically the two areas of the objects combined as it describes the sum of each of the possible reactions for a Nucleus and it constitutes the probability of the reaction occurring. However, nuclear reactions are governed by quantum mechanics thus the cross section is not described geometrically and instead is described as:

$$\sigma = \pi \bar{\lambda}^2 \tag{11}$$

Where $\bar{\lambda}$ stands for the de Broglie wavelength and /sigma stands for the cross section [35].

We have to also consider the repulsive force of the positively charged protons. The colliding particles can be modelled as two spherical objects with point charges equivalent to the charge of a proton multiplied by the number present in each nuclei. This allows us to calculate the energy required for them to actually collide and be close enough to overcome the nuclear strong force, which becomes attractive rather than repulsive once particles are close enough.

The Coulomb barrier is the barrier to two particles of the same charge colliding caused by their repulsion of each other. It can be written as:

$$V_c = \frac{e^2}{4\pi\varepsilon_0} . \frac{Z_a Z_b}{R_a + R_b} \tag{12}$$

where Z is the atomic number of each nuclei involved and R is the radius of the respective nuclei. (Equations 12-16 [36]).

If we now consider a stellar gas, usually the nuclei will be moving non-relativistically and the gas should be in thermal equilibrium. As such the range of velocities and thus kinetic energy of the individual nuclei should be able to be described according to the Maxwell-Boltzmann velocity distribution. As there are two particles colliding in this instance an equation describing the potential velocity of particle x and particle y is required.

$$\phi(v_x) = 4\pi v_x^2 \left(\frac{m_x}{2\pi kT}\right)^{\frac{3}{2}} exp\left(\frac{-m_x v_x^2}{2kT}\right) \tag{13}$$

$$\phi(v_y) = 4\pi v_y^2 \left(\frac{m_y}{2\pi kT}\right)^{\frac{3}{2}} exp\left(\frac{-m_y v_y^2}{2kT}\right) \tag{14}$$

Essentially the Maxwell-Boltzmann distribution here is describing the probability that a particle within the gas will have a given velocity depending on the energy of the gas overall.

$$\langle \sigma v \rangle = \int_0^\infty \int_0^\infty \phi(v_x)\phi(v_y)\sigma(v) v dv_x dv_y \tag{15}$$

Using this information and $E = \frac{1}{2}\mu v^2$ we can write the cross section for a particle pair reaction as:

$$\langle \sigma v \rangle = \left(\frac{8}{\pi\mu}\right)^{\frac{1}{2}} \frac{1}{(kT)^{\frac{3}{2}}} \int_0^\infty \sigma(E) E\, exp\left(-\frac{E}{kT}\right) de \tag{16}$$

This equation (equation 16) shows the general formula for the reaction rate per particle pair.

5.2.1 Stellar Reaction Rates

If particles were required to have kinetic energy sufficient to overcome the coulomb barrier, as described in equation 12, then the temperature required for fusion of even the smallest elements would be far higher and result in lower abundances of elements in stars than we observe; in fact the differences in reaction rates could well be enough that we wouldn't even exist.

In reality, the fusion reactions can begin to occur at lower temperatures than the temperature that would be required for the particles to have sufficient kinetic energy to overcome the coulomb barrier. This is because of a phenomenon in quantum mechanics called "quantum tunnelling" and is a result of the dual nature of particles, it arises from their wave nature. Quantum tunnelling is described as being the probability that a particle, when presented with a barrier it lacks the energy to penetrate according to classical physics, will none the less pass straight through. This probability can be described as [37]:

$$P = exp{-2KR_c}\left[\frac{arctan(R_c/R_n - 1)^{\frac{1}{2}}}{(R_c/R_n - 1)^{\frac{1}{2}}} - \frac{R_n}{R_c}\right] \tag{17}$$

where:

$$K = \left[\frac{2\mu}{\hbar^2}(E_c - E)\right]^{\frac{1}{2}} \tag{18}$$

Taking into account the fact that the probability of a particle penetrating the coulomb barrier approaches 1 as the kinetic energy of the particles approaches that of the coulomb barrier. However, for lower temperatures it drops off rapidly. The expression for the probability tunnelling will occur is commonly called the "Gammow Factor". It can be written as:

$$P = exp(-2\pi\eta) \tag{19}$$

Taking this into account and using the astrophysical S factor- which basically represents all the strictly nuclear effects [38]. You can combine these with Equation 16 to get a general equation for the non resonant stellar reaction rate per particle pair:

$$\langle\sigma v\rangle = \left(\frac{8}{\pi\mu}\right)^{\frac{1}{2}} \frac{1}{(kT)^{\frac{3}{2}}} \int_0^\infty S(E)\ \left[exp - \frac{E}{kT} - \frac{b}{E^{1/2}}\right] \tag{20}$$

5.2.2 Resonant Reaction Rates

The reaction rate per particle pair for a stellar reaction can be described as [37] :

$$\langle\sigma\upsilon\rangle = \left(\frac{8}{\pi\mu}\right)^{\frac{1}{2}} . \frac{1}{(kT)^{\frac{3}{2}}} \int_0^\infty \sigma_{BW}(E) E\ exp\left(-\frac{E}{kT}\right) dE \tag{21}$$

Where σ_{BW} is the Breit-Wigner cross section.

$$\langle\sigma\upsilon\rangle = \left(\frac{8}{\pi\mu}\right)^{\frac{1}{2}} \frac{1}{(kT)^{\frac{3}{2}}} E_R\ exp\left(-\frac{E_R}{kT}\right) \int_0^\infty \sigma_{BW}(E) dE \tag{22}$$

$$\int_0^\infty \sigma_{BW}(E)dE \;=\; \pi\lambda_R^2\omega\Gamma_a\Gamma_b\int_0^\infty \frac{1}{(E-E_R)^2+\left(\frac{\Gamma}{2}\right)^2}dE \;=2\pi^2\lambda_R^2\omega\frac{\Gamma_a\Gamma_b}{\Gamma} \tag{23}$$

where the product of the width ratio γ and the statistical factor ω is:

$$\omega\gamma = \omega\frac{\Gamma_a\Gamma_b}{\Gamma^2} \tag{24}$$

when ω is determined by the relationship between the spins of the reaction channels:

$$\omega = \frac{2J+1}{(2J_1+1)(2J_2+1)}(1+\delta_{12}) \tag{25}$$

The Resonance Strength $\omega\gamma$ refers to the integral of the cross section of the reaction. The maximum resonance cross section σ_R is found when $E = E_R$. δ_{12} is the probability that the associated sub-states will be occupied.

$$\sigma_R = \sigma(E=E_R) = 4\pi\lambda_R^2\omega\frac{\Gamma_a\Gamma_b}{\Gamma^2} \tag{26}$$

so combining equations 22,24,25 and 26 gives the stellar reaction rate per particle for a narrow resonance.

$$\langle\sigma\upsilon\rangle = \left(\frac{2\pi}{\mu kT}\right)^{\frac{3}{2}}\hbar^2(\omega\gamma)_R\, exp\left(-\frac{E_R}{kT}\right)f \tag{27}$$

5.3 Triple Alpha Process

The triple alpha process, refers to a potential fusion pathway that allows for the formation of carbon from helium [39].

$$^4He + ^4He \rightleftharpoons ^8Be \tag{28}$$

$$^8Be + ^4He \rightleftharpoons ^1\,^2C \tag{29}$$

It gets it's name "the triple alpha process" from the fact that essentially it is 3 alpha-radiation clusters of nucleons (a helium nucleus- 2 protons and 2 neutrons) fusing to form Carbon-12 in a 2 step process. This process can be seen in equations 23 and 24.

5.3.1 The Hoyle State

The Hoyle state is a specific excited state of carbon that has a chance of decaying to form a stable carbon-12 isotope. This formation pathway is an example of formation via a narrow resonance which was previously described and equation 27 shows the formula for the reaction rate per particle pair for a narrow resonance. It forms primarily through formation of a 0^+ excitation state of the carbon 12-nucleus; however, it can form via a second pathway that involves a 2^+ formation pathway. The Hoyle state is actually theorised to in-fact be another state of matter, rather like a Bose-Einstein condensate [40]. It is thought that whilst in its excited form prior to decay back to beryllium-8 or decay to a stable carbon-12 atom that it exists as 3-bound alpha particles. Bound

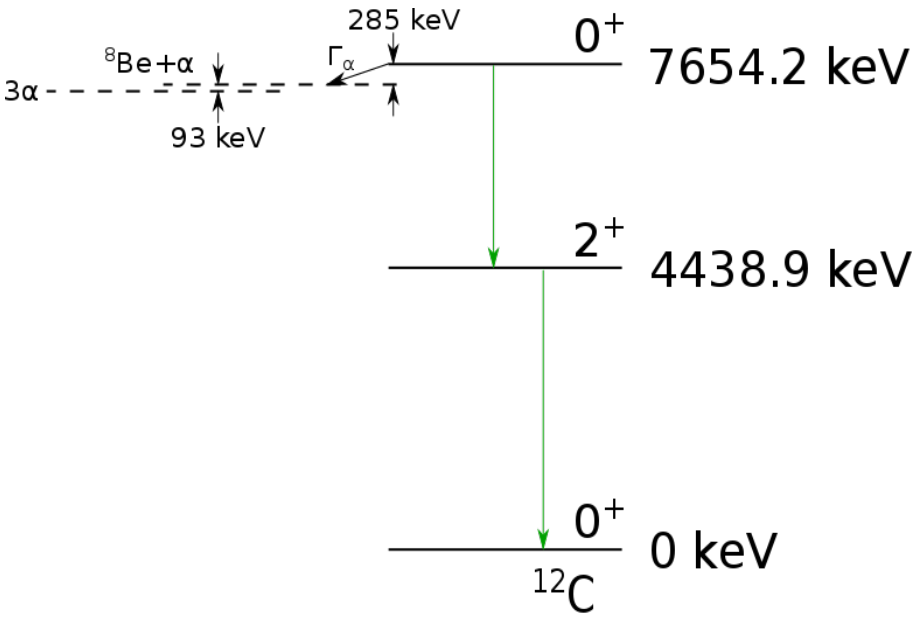

Figure 7: diagram showing the most common decay pathways for the Hoyle state [6].

together but still in 3 distinct clumps of nucleons. The decay pathways for the Hoyle state are either through 2 gamma-ray decays ($0^+ \Rightarrow 2^+ \rightarrow 0^+$) and decay via e^+e^- pair production ($0^+ \rightarrow 0+$) The excited energy of the Hoyle state carbon 12 nucleus is 7.65MeV and the 2+ intermediate state is 4.43MeV. The Hoyle state is so important because if it didn't exist with the specfic decay widths it has, then the Carbon to oxygen ratio in the universe (about 0.6) would be different and that would completely change the evolution of the universe, specifically with respect to life like us being able to exist [12]. The reaction rate of the Hoyle state is [36]:

$$\langle \sigma v \rangle \propto \frac{\Gamma_\alpha \Gamma_{rad}}{\Gamma} \, exp(-E_R/k_B T) \tag{30}$$

Where $\Gamma + \alpha$ is the chance decay back to beryllium-8, Γ_{rad} is the radiative width of the decay to the stable form of carbon-12 and comprises the width of both of the possible decay pathways down to a stable carbon-12 atom. [41].

The full reaction rate for carbon-12 formation via the narrow resonance known as the Hoyle state and the equation I used to calculate my reaction rate is as follows [42]:

$$N^2{}_A \langle \alpha\alpha\alpha \rangle = 3^{\frac{3}{2}} 6 N_2^2 \left(\frac{2\pi\hbar^2}{m_4 k_B T} \right)^3 \frac{\Gamma_{rad}}{\hbar} \, exp(-Q/k_B T) \tag{31}$$

6 Methods

In order to investigate the effect that the new value for Γ_{rad} would have upon current nucleosynthesis models for a neutron star in a common envelope binary system, I had to establish the current state of research regarding nucleosynthesis of carbon-12 and how the reaction rates are derived. I initially started by replicating some calculations for established reaction rates for some other elements that have plenty of observational data to confirm the accuracy of those rates. This also helped me to practice producing some results based on rates in the reaction library used by NuGrid. (For the avoidance of doubt, beyond contributing to my understanding that then formed the background section of this work, any graphs etc produced here aren't relevant to the results of my research and as such aren't included in any part of this thesis.) Once I had established a decent understanding of the background theory I was ready to move onto calculating the reaction rate for the resonant reaction using the new value for Γ_{rad}. I did this by writing some python code and the code is included in appendix A. I then compared this to calculations made also using my code but with the previously accepted value for Γ_{rad} and with previous reaction rate calculations; that take into account not just the resonant reaction rate for the Hoyle state but also other non-resonant reaction pathways for the formation of Carbon-12. At the temperature range I was interested in (roughly 0.1 Giga-kelvin through to 2.0 Giga-kelvin) the resonant reaction rate should be the dominant method for Carbon-12 formation. Figure 8 contains a plot showing my reaction rate for values up to 2 Giga-kelvin.

Following this analysis I worked on applying this reaction rate as best I could in NuGrid. I began by running simpler simulations as benchmarks for a solar environment at a constant temperature and pressure and compared the outputs to one another. I then did the same for a Helium rich environment where over 95 percent of the initial abundance of elements are Helium Nuclei. I then moved on to using trajectories obtained from others in the research group (Chris Fryer) who has been running Hydrodynamic Simulations to model common envelope binary systems. S Hydrodynamic simulation is a , computationally intensive process that aims to simulate the flows of different fluids and their interactions with one another. They are often used as a model to simulate the interaction of fluids and the flows within the fluid. One common use is in large-scale simulations of systems in astrophysics as the interactions of particles in a range of scenarios often referred to as 'astrophysical fluids' such as the formation of a star. Due to constraints on the mean free path for systems involving the collision of particles, the ideal fluid description of matter that hydrodynamic simulations are based upon, can be adopted to model such gas-dynamical scenarios in astrophysics. The simulations work by solving three-dimensional Euler-Equations[43].

Chris Fryer has been looking at accretion onto a black hole using hydrodynamical simulations however some of the results from his simulations can also be applied to a Neutron star up until the point where it would merge with the donor stars core if it isn't ejected from the envelope. The data from the simulations provides data on the temperature and pressure at various times throughout the simulation. These can be listed and become the trajectories I use to analyse the reactions using NuGrid. The trajectories are essentially a list of times and a corresponding temperature and pressure at that time.

I had trajectories for a range of different accretion rates for a neutron star with a mass of 2.0 solar masses. I chose this mass as it is realistic mass for a neutron star as evidenced by figure 3, it's a similar mass to J1614-2230 as indicated on the graph. Using figure 3 as a reference point, it indicates that the various models for a neutron star's composition would make it unlikely to have a radius of 10km or less. As such I have stuck to using minimum radii for the distance between the centre of the Neutron star and the core of the donor star that are greater 10km. I used values for the minimum radius 11.112km and 13.869km. I chose these because again in reference to figure 3 I notice most of the models tend to cluster where they would result in radii between 11 and 14km so it made sense to me to choose values at either end, that way they should bear some resemblance to reality for helium burning on the surface of a neutron star.

6.1 New Reaction Rate for Carbon-12 formation Via the Hoyle State

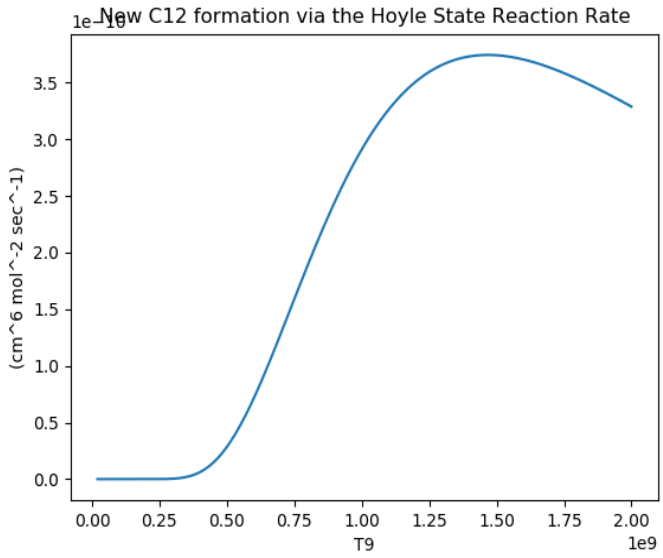

Figure 8: Graph showing plot of my new reaction rate for Carbon-12

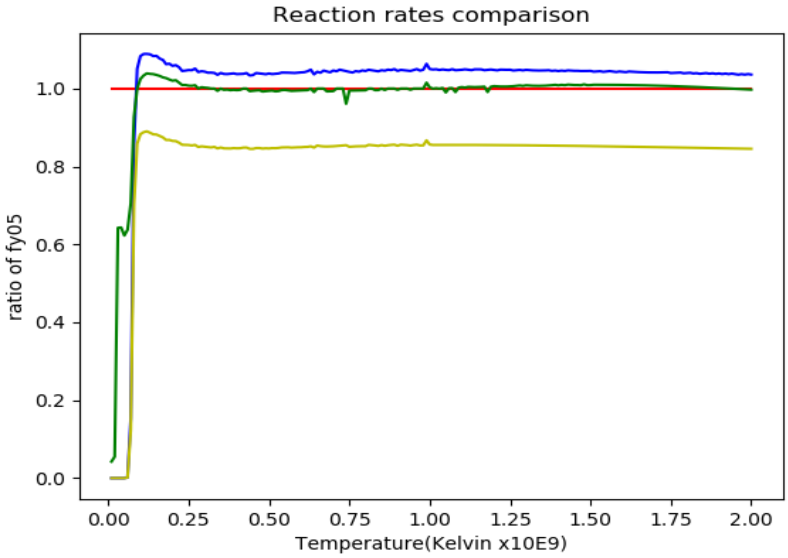

Figure 9: Graph Showing my New reaction rate(blue), the reaction rate calculated using the old value for Γ_{rad} (yellow), cf88 [7] rate(green) and fy05 rate [8] (red) all as a ratio of fy05. The rates are named after the primary authors of the respective papers they came from.

As can be seen in figure 9 my new reaction rate calculation comes out significantly higher than the rates fy05[8] and cf88 [7]. Both fy05 and cf88 include a contribution towards the rate from non-resonant processes however whereas the calculation using the old value of Γ_{rad} does not include these contributions and considering the new value of Γ_{rad} is 34 percent higher than the previously accepted value, the fact that my rate is approximately 30 percent higher is an indication that as expected the new value for Γ_{rad} should have a significant effect on nucleosynthesis models as I will explore later. The difference between my new rate and the same calculation run using the old value for the radiative width helped me to determine how best to assess this change in NuGrid. Due to the way NuGrid works you cannot typically implement a new reaction rate, instead it makes more sense to use a scaling factor on the existing rate that NuGrid is using. I went with a 30 percent increase because that is roughly the same increase seen between rates and should allow me to assess if the increase is enough to substantially effect the nucleosynthesis models, I will be assessing the effect it has; specifically in the temperature range where the triple alpha process should dominate synthesis of carbon-12.

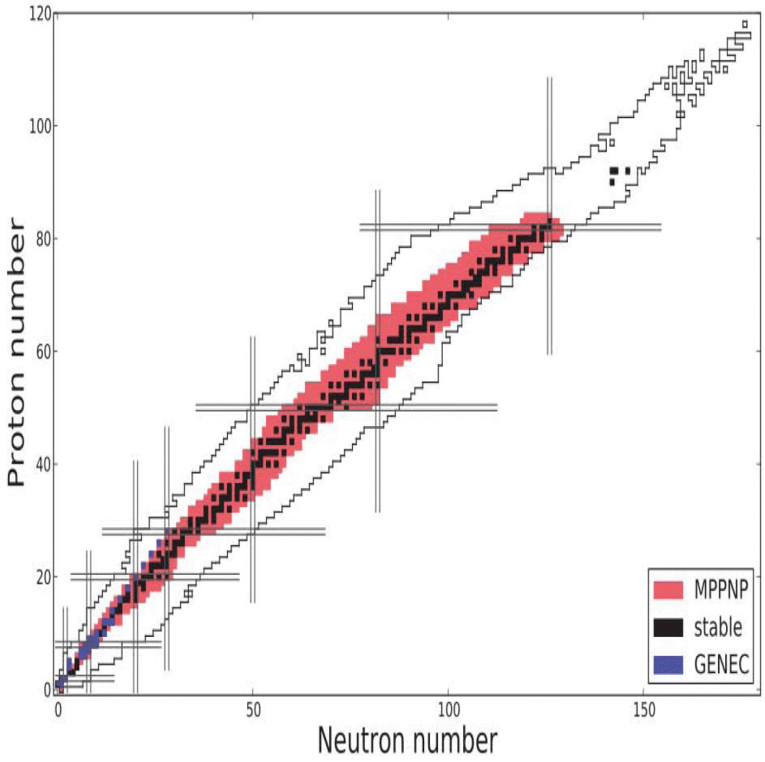

Figure 10: Shows the reactions covered by PPN (single zone post processing network) and MPPN (multiple zone most processing network) and other parts of the NuGrid software [9].

6.2 NuGrid: Post Processing Code/Tools

NuGrid stands for ”The Nucleosynthesis Grid Collaboration”. The collaboration is the work of a number of scientists from a variety of countries around the world, collaborating and sharing research on astrophysics and/or Nuclear physics/chemistry via the NuGrid software framework [44] in order to keep the simulation software up to date . They contribute knowledge and code to the code-base and share their results with the wider community which enables improvements to be made to the software, it is designed to be easily accessible and to use less processing power than running whole hydro-dynamical simulations.

At a fundamental level it uses large networks of reaction rate libraries to simulate the outputs in terms of abundance of various elements and their different isotopes at various different time steps. You have a variety of options such as whether to complete a run with a constant temperature and pressure, how long you want it to simulate for and you can change the initial abundance files that set the abundance of each isotope at the start of the simulation depending on the scenario you are interested in. I started with some basic benchmarks to show how the reactions compare to one another for a solar environment and how they compared to similar simulations for a helium rich environment. You can also ask NuGrid to exclude particular reactions or include additional processes as may be relevant to the scenario investigated. You can also set it up to run pre-set trajectories; files that include timesteps and the temperature

and pressure at each time step and some other parameters.

The bulk of my results come from simulations run using trajectories I acquired from Alex Hall-Smith who in turn had received them from Chris Fryer. As previously mentioned Chris Fryer has been running hydrodynamic simulations to simulate accretion of material onto a black hole and other Astrophysical phenomena [45]. I based my simulations on the trajectories with a minimum radius corresponding to the potential radii allowed for a neutron star of 2 solar mass as previously discussed. Chris's simulations were aimed at simulating the the conditions that might occur (in terms of temp and pressure) when material accretes onto a blackhole. However, as prior to the instant at which the core and neutron star merge and then collapse inwards to form a black hole, the physics in terms of the conditions (temperature and pressure at different accretion rates) remains the same for scenarios like mine- a late stage red giant with a Neutron star orbiting it and eventually entering it's gas cloud and taking material from it through accretion and then fusing that material. Single zone post processing is less computationally intensive than the multi-zone post processing. The single zone takes the trajectory file and uses the physics solver to reduce the reaction network down to only those reactions that can occur under the conditions indicated by the trajectory file, e.g:the temperature and pressure. Each particle is not followed individually however the code does ensure that the number of particles is roughly conserved to within a certain degree of tolerance, which means the yields it acquires can be relied upon to be broadly accurate. It assumes no mixing of material between zones. The key difference between the Multi zone-post processing network and the single zone post processing network is that the latter can simulate scenarios where there is mixing of material between zones.

I used the single-zone post-processing network as it is considered unlikely there would be mixing between the zones in the scenario I was researching. [28] This meant it was best suited for my purpose; changing the scaling factor on an individual reaction, carbon-12 formation from 3 helium nuclei-otherwise known as the triple alpha process. The reaction library used was jinareaclib [46] which means the default rate that the triple alpha process should have had before I applied a scaling factor would have been the fy05 rate. Figure 11 is a diagram that shows the primary processes and use for PPN and MPPN. PPN operates and how it's designed to be used compared to the MPPN, which uses thousands of networks and is better designed for looking at larger scale events from more of an Astrophysical macroscopic perspective. A number of python based tools including a specific module for using python to interpret and present data outputs from NuGrid.

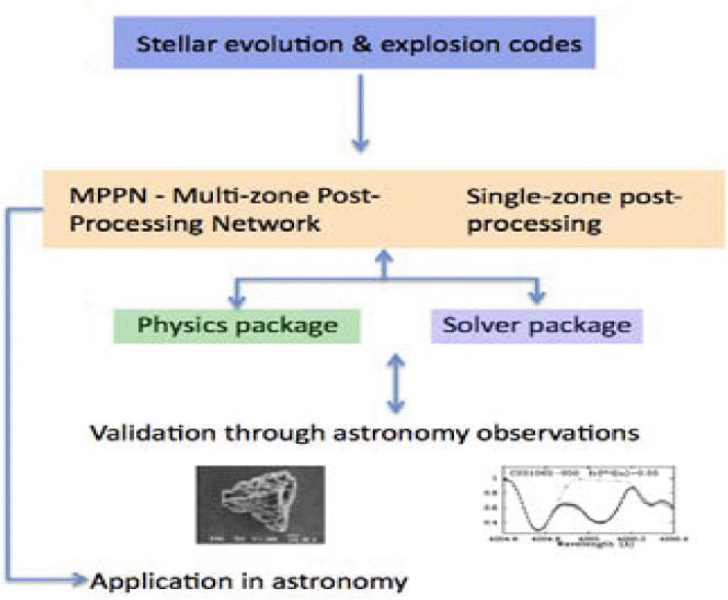

Figure 11: Diagram showing the different ways NuGrid can process data and how that applies to Astronomy/Astrophysics. [10].

7 Results and Analysis

In this section I will present the data that I collected using NuGrid to establish how much of an effect a new reaction rate; roughly 30 percent higher than the previous accepted rates appears to have on the Nucleosynthesis models. Specifically on the rate of Carbon-12 formation and the potential impact this has on the abundance of carbon the formation of other, heavier elements like oxygen.

7.1 Benchmarks

To begin with I ran some basic simulations using NuGrid, no trajectories just a constant temperature and pressure and I started using initial abundances for a solar environment.

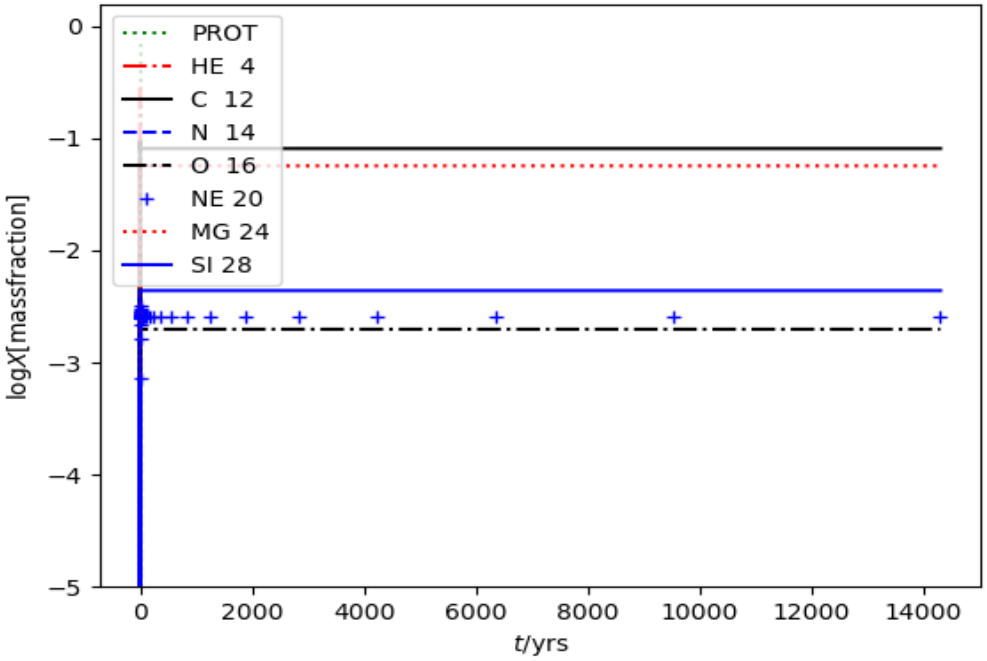

Figure 12: Log of the mass fraction of some isotopes such as hydrogen/protons,helium,carbon,oxygen vs the time . This is for a constant T= 0.5 Giga-Kelvin with a constant density of 1.62 g/cm^3

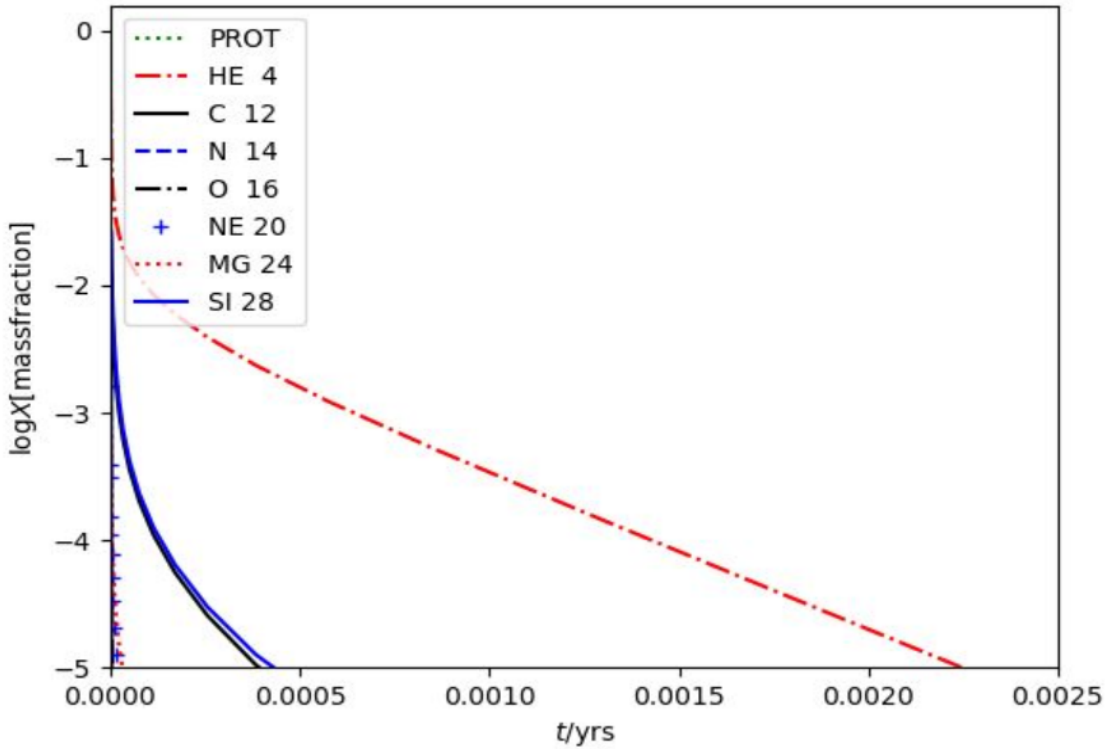

Figure 13: Log of the mass fraction of some isotopes such as hydrogen/protons,helium,carbon,oxygen vs the time . This was for T= 1.0 Giga-Kelvin with a density of 1.62000 g/cm^3

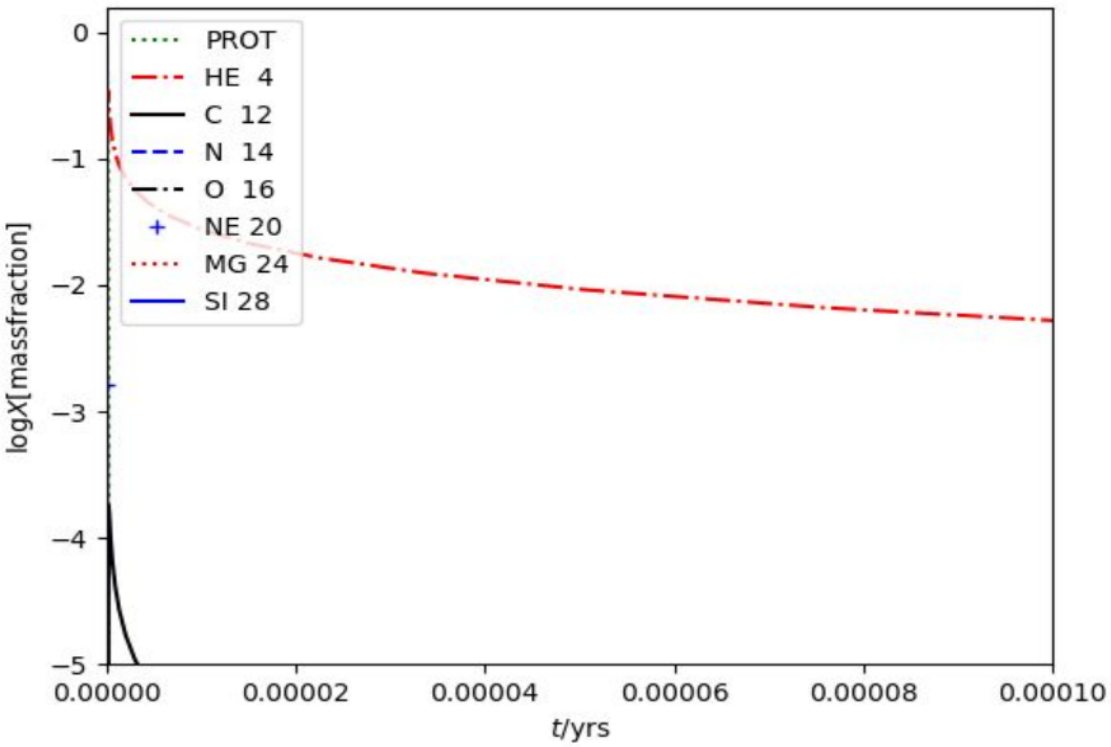

Figure 14: Log of the mass fraction of some isotopes such as hydrogen/protons,helium,carbon,oxygen vs the time . This was for T= 2.0 Giga-Kelvin with a density of 162000 g/cm^3

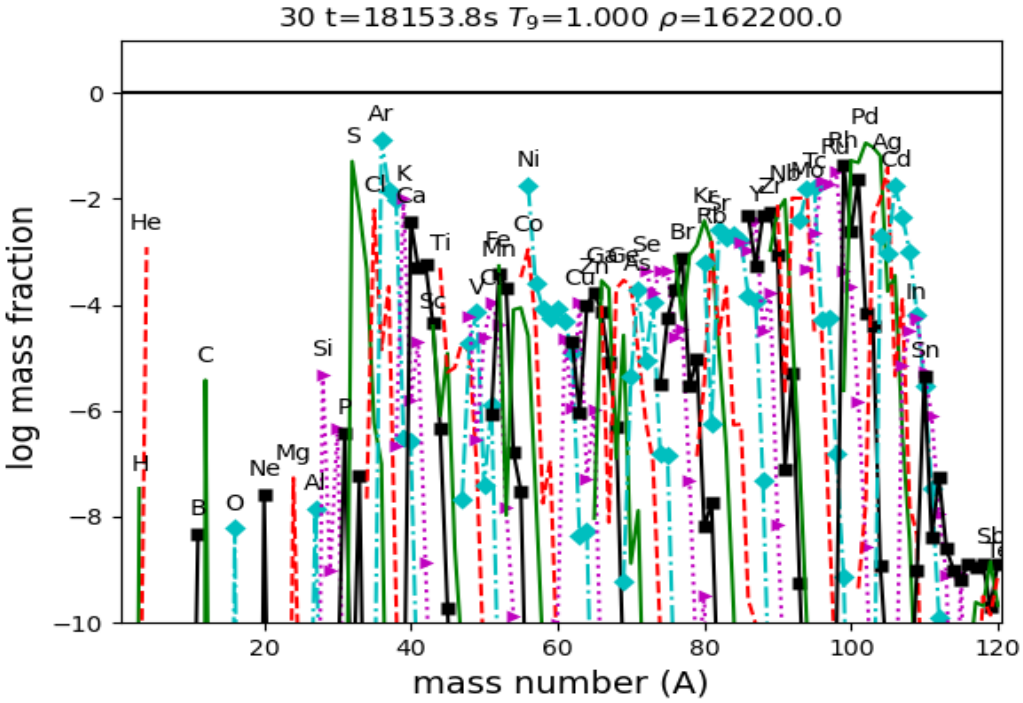

Figure 15: Shows the abundances of the elements present at the time 18153.8 seconds for the scenario shown in figure 15.

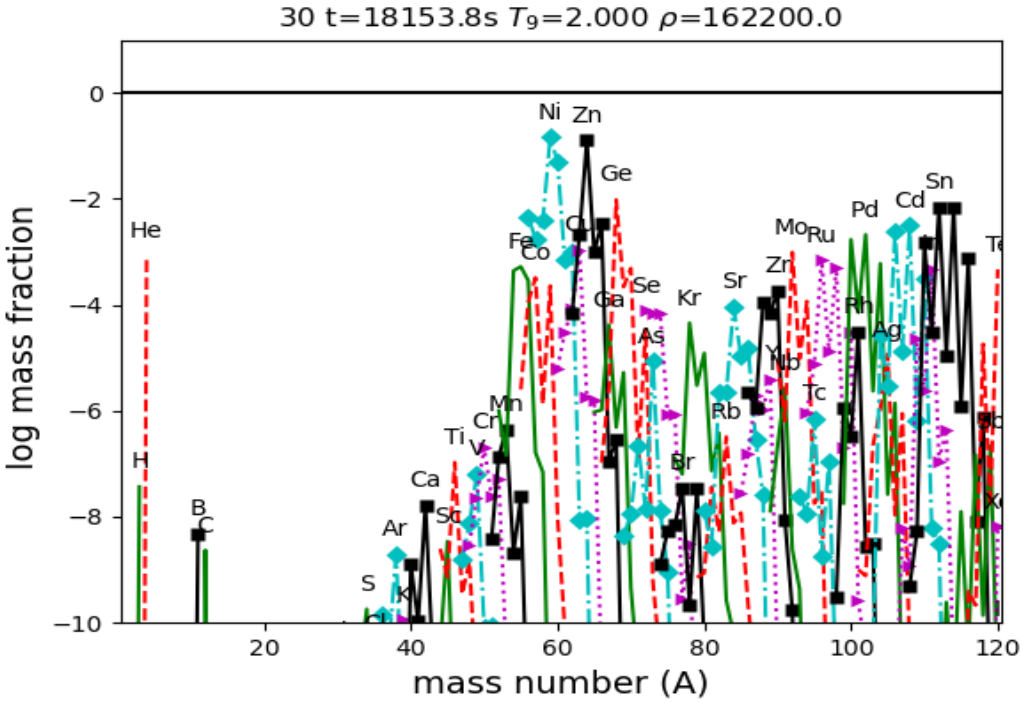

Figure 16: Shows the abundances of the elements present at the time 18153.8 seconds for the scenario shown in figure 16.

As can be seen in figures 12, 13 and 14. The only thing that changes between them is the temperature and whilst the temperatures examined aren't particularly realistic for a solar burning scenario the purpose was merely to demonstrate the kind of change the temperature would have upon the outputs. In each instance fusion occurs rapidly for lighter isotopes and quickly moves on to fusing heavier isotopes, the hotter it is, the more rapidly and efficiently that appears to occur, with few of the lighter isotopes left at all in the 2 giga-kelvin scenario. This is further demonstrated in figure 15 and 16 which are abundances from the same time-step in the 1 gigakelvin and 2 gigakelvin scenarios respectively and a clear shift to the right (heavier isotopes) can be seen in figure 16. Again it's worth pointing out these are not realistic scenarios, I was simply assessing how changing the inputs would effect the outputs.

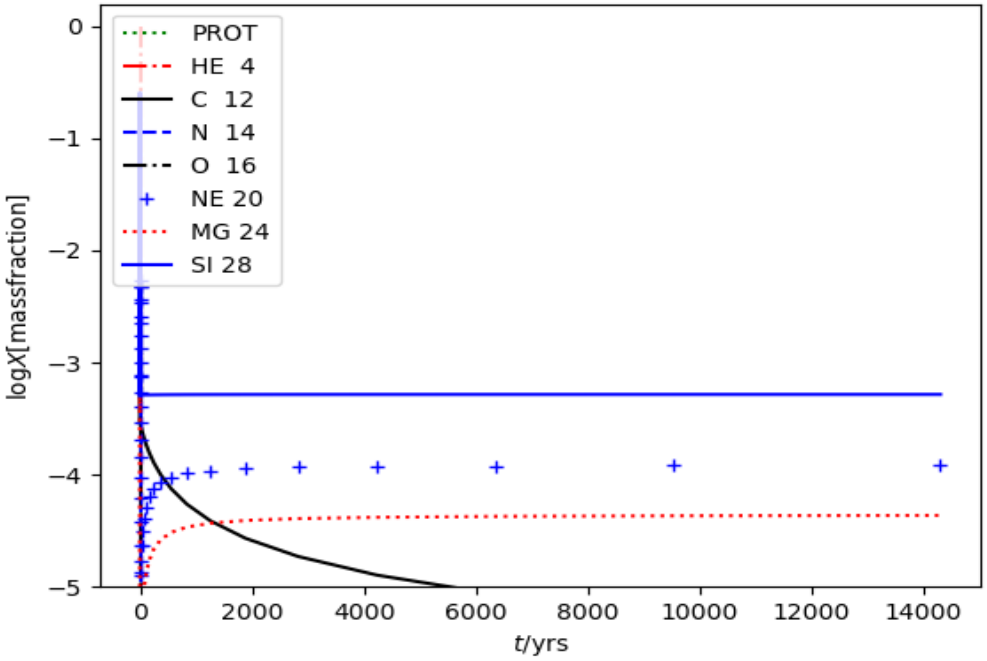

Figure 17: Shows plots for Hydrogen to Silicon over time for a Helium rich environment at 1 gigakelvin with a density roughly that of the outer regions of the sun (162000 g/cm^3

.

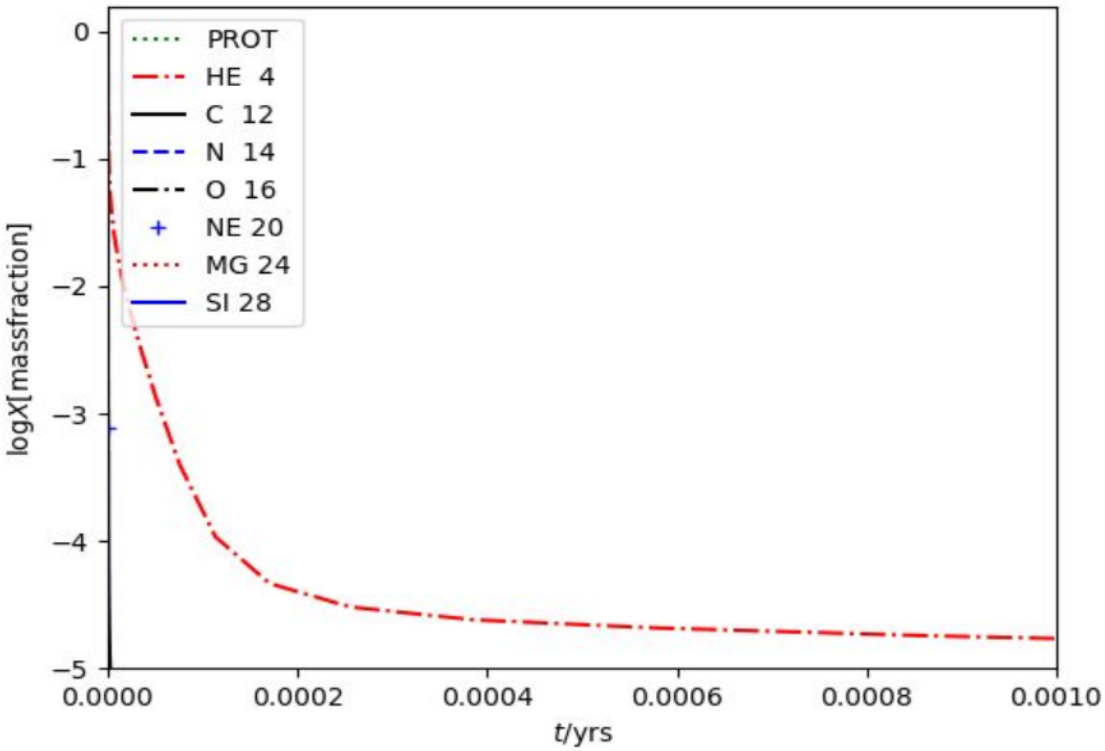

Figure 18: Shows plots for hydrogen to silicon over time for a helium rich environment at 2 gigakelvin with a density roughly that of the outer regions of the sun (162000 g/cm^3).

Figures 16 and 17 now show a helium rich environment-like that in a late stage red giants gas cloud- for the same stable lighter isotopes: hydrogen, helium-4, carbon-12, nitrogen-14, oxygen-16, neon-20, magnesium-24 and silicon-28. All chosen because they are isotopes who's abundance in a Helium burning scenario should be directly impacted by the rate at which carbon-12 forms.

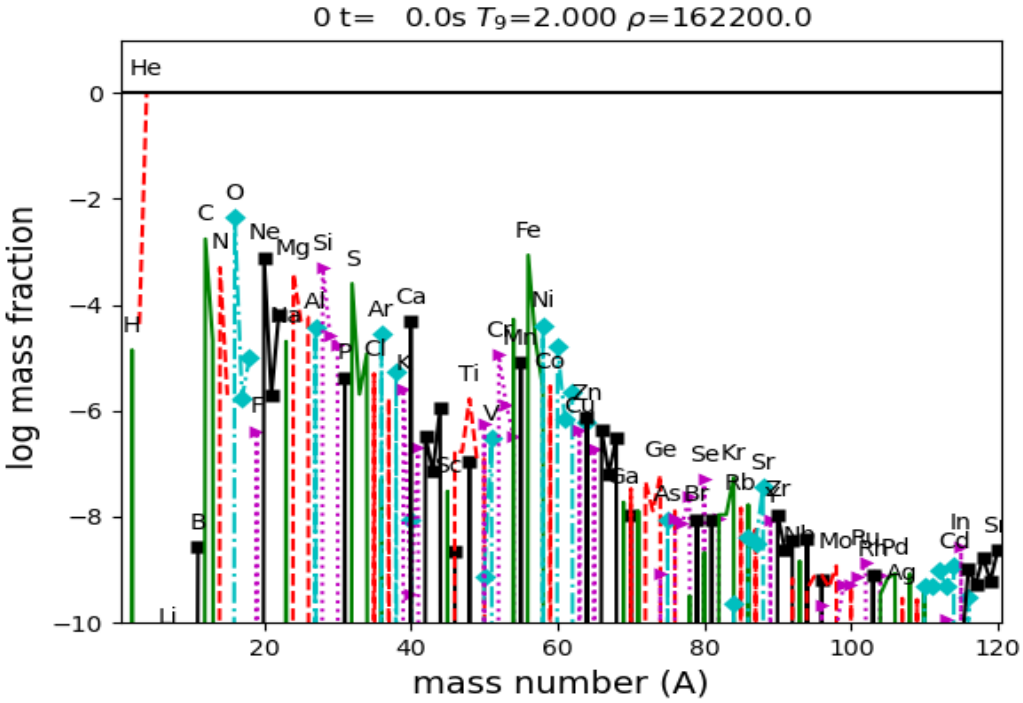

Figure 19: Shows the initial solar abundances [11] with the Hydrogen mostly replaced by Helium to simulate a helium rich environment for the 45 lightest isotopes for a helium rich environment.

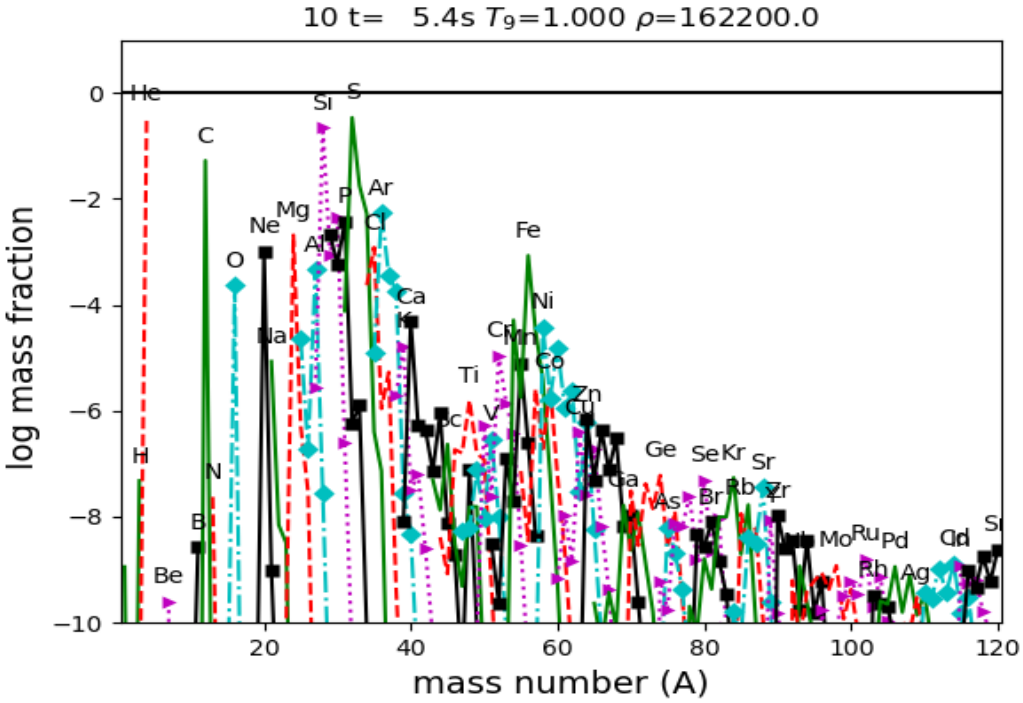

Figure 20: Shows the lightest 45 isotopes and their abundance at 5.4 seconds for a density of 162200gcm^{-3} which is roughly equivalent to the density of the sun and a temperature of 1 gigakelvin.

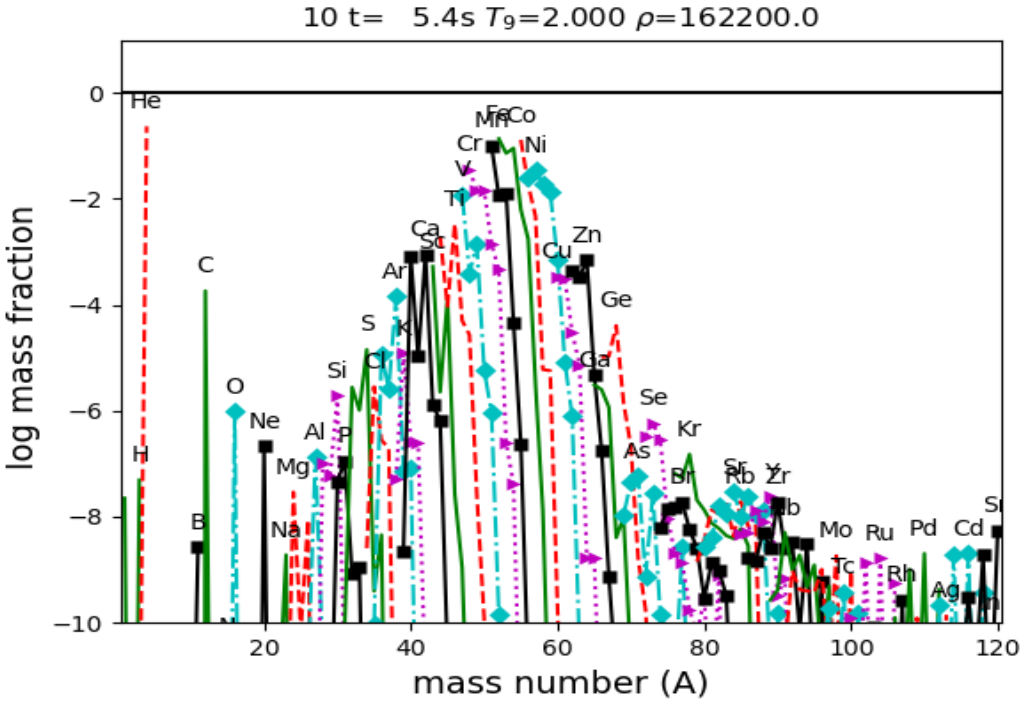

Figure 21: Shows the lightest 45 isotopes and their abundance at 5.4 seconds for a density of 162200gcm^{-3} roughly equivalent to solar density and a temperature of 2 gigakelvin.

The purpose of these figures is to assess how the temperature effects helium burning and specifically the effect on the abundance of carbon-12. Figure 19 shows the initial abundance for a Helium rich environment and contrasting figure 22 and figure 21 with the initial abundance shown in figure 19. You can see in figure 20 a large amount of carbon being produced, whereas in the higher temperature scenario shown in figure 21, there is considerably less carbon than in there was figure 19 and a clear shift to the right in terms of the most abundant isotopes which suggests that the high temperatures means carbon is already fusing to form heavier isotopes and would suggest that the window for triple alpha boosting the production of carbon has been exceeded. It should sit at somewhere between the 1 - 2 gigakelvin mark.

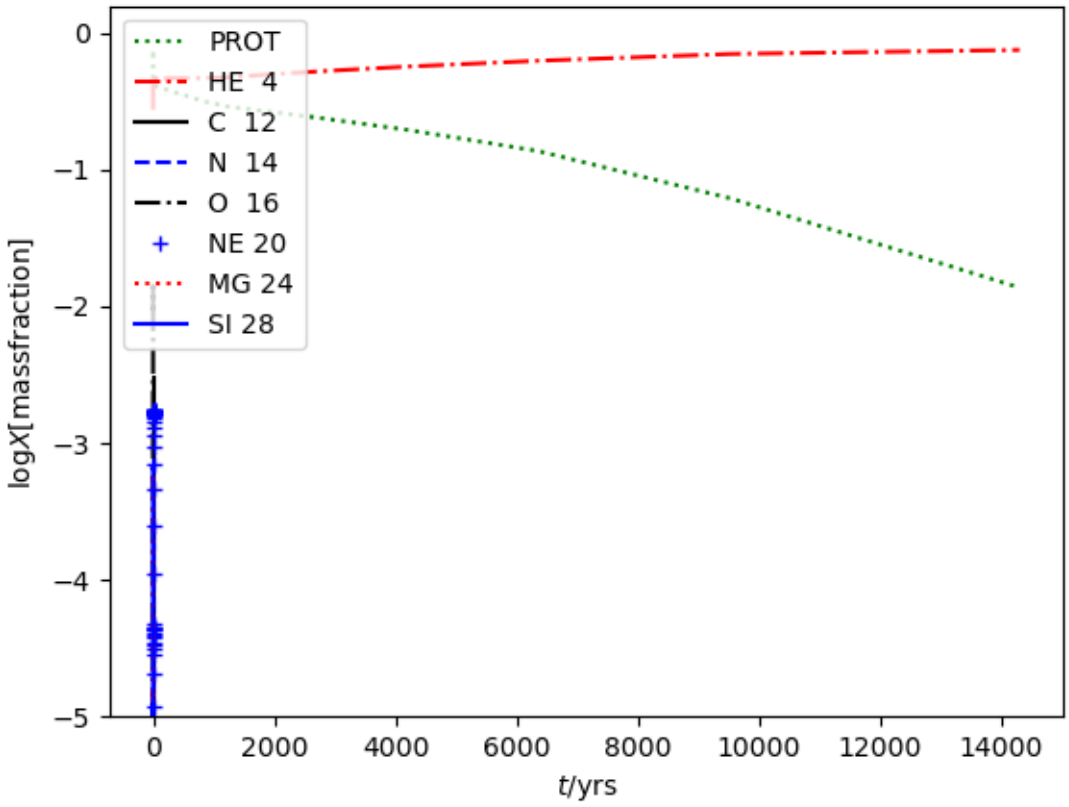

Figure 22: Shows the change in abundance over time of the same selection of light isotopes as shown in figure 20, at a constant temperature and density of 1 gigakelvin with a density 0.001 grams per cm^3

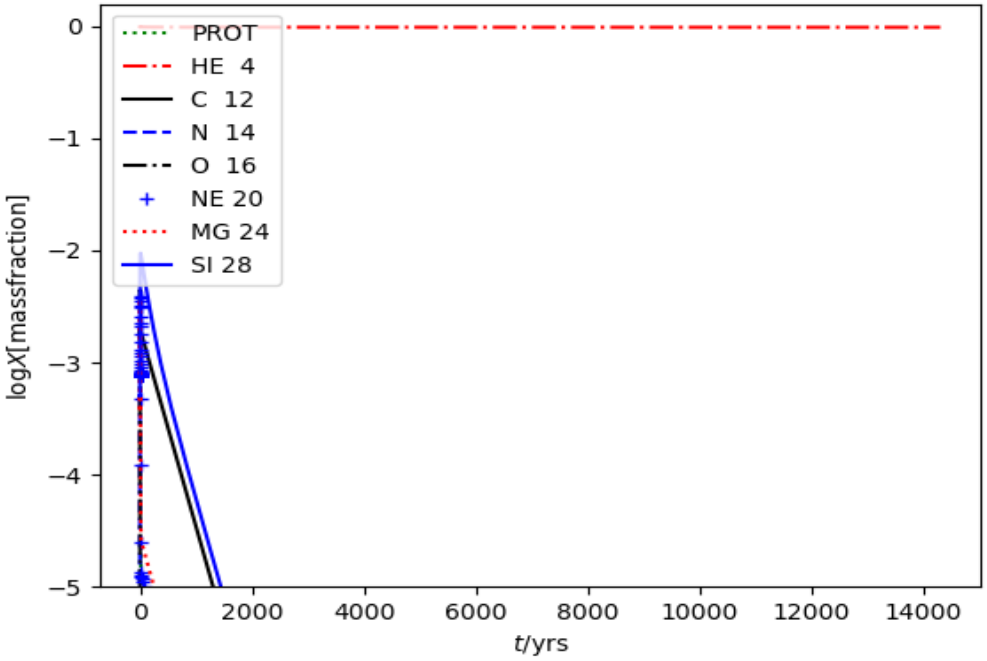

Figure 23: Shows the change in abundance over time of the same selection of light isotopes at a constant temperature and density of 1 gigakelvin with a density 0.0001 grams per cm^3

.

Figure 22 and 23 compare the effect that density has on the formation of carbon-12 via the triple alpha process. The nature of the reaction; the fact it has two parts to it means I would expect density to have a greater effect on the reaction rate than temperature. As you can see the lower density scenario in figure 23, some fusion occurs at the start but then as the process progresses the number of protons remains high and is actually higher than at the start. Meanwhile, figure 22 shows rapid fusion (as seems to be characteristic of the constant temp and pressure reactions vs a trajectory with highly variable rates) and the helium and hydrogen clearly deplete fully and much more rapidly. In figure 23 you can see the carbon, hydrogen, neon, et cet era steadily deplete. Presumably they are reacting with one another to form heavier elements. The same process should have occurred in both instances only it can be better observed in figure 23 due to the lower density of 1 order of magnitude (x10) which slows down the process, meaning on graphs covering these time spans it becomes more visible.

7.2 Rate comparisons

The next section will show the results of the trajectories (lists of temperatures and density's at various times) for both the current accepted reaction rates calculated using the old value of Γ_{rad} and with the scaling factor increased by 30 percent to approximate the effect the new value of Γ_{rad} has on the reaction rate.

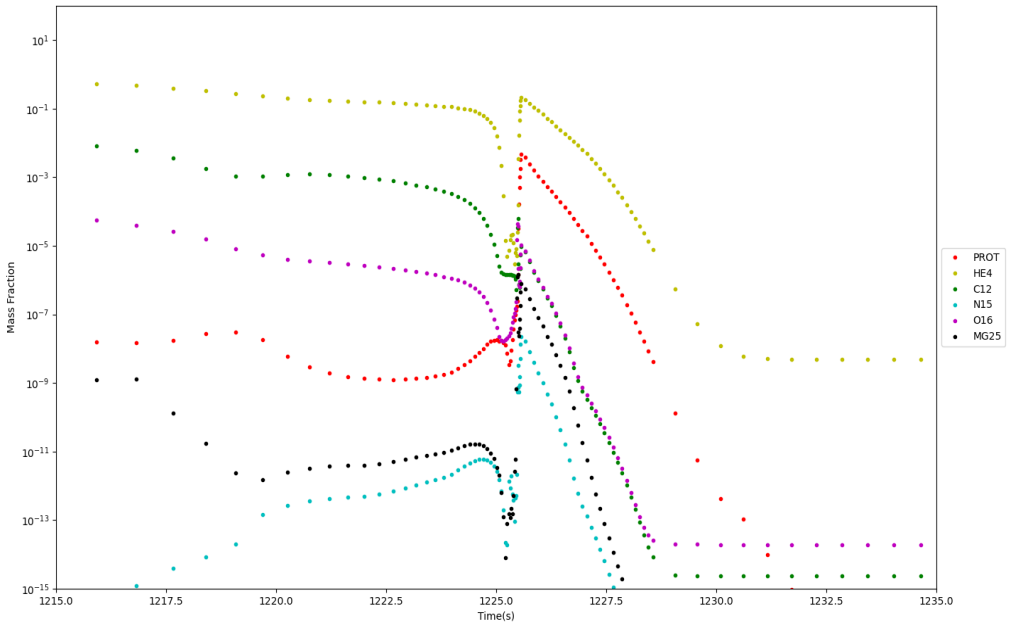

Figure 24: With the old reaction rate; The mass fraction over time for accretion rate of 64x10^{-5} solar mass per second and a minimum radius of 13.86km.

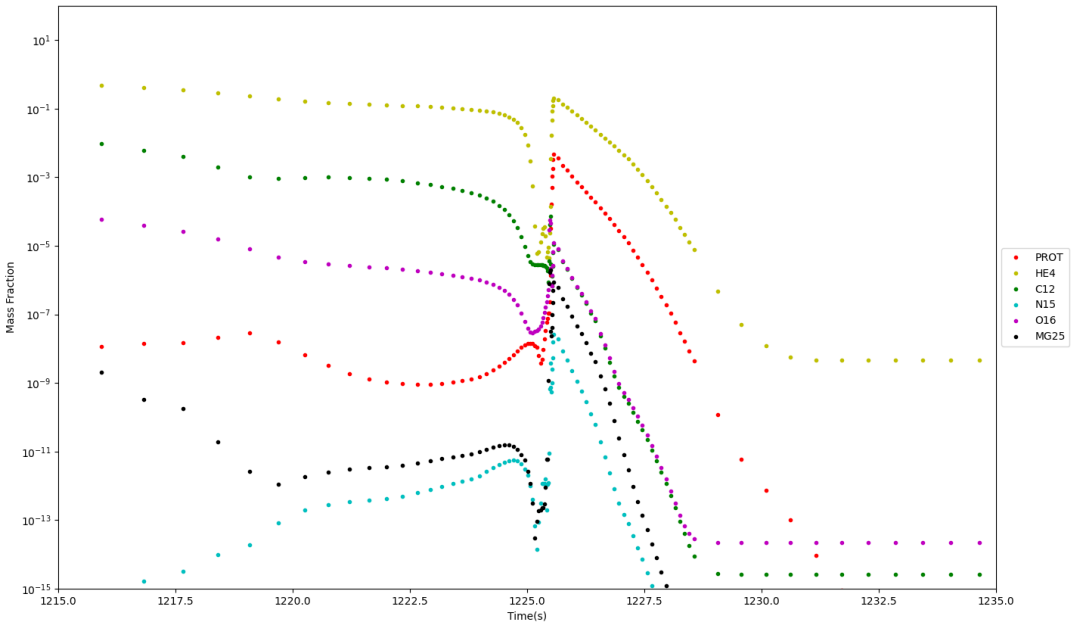

Figure 25: With the scaling factor applied; the mass fraction over time for accretion rate of 64x10^{-5} solar mass per second and a minimum radius of 13.86km.

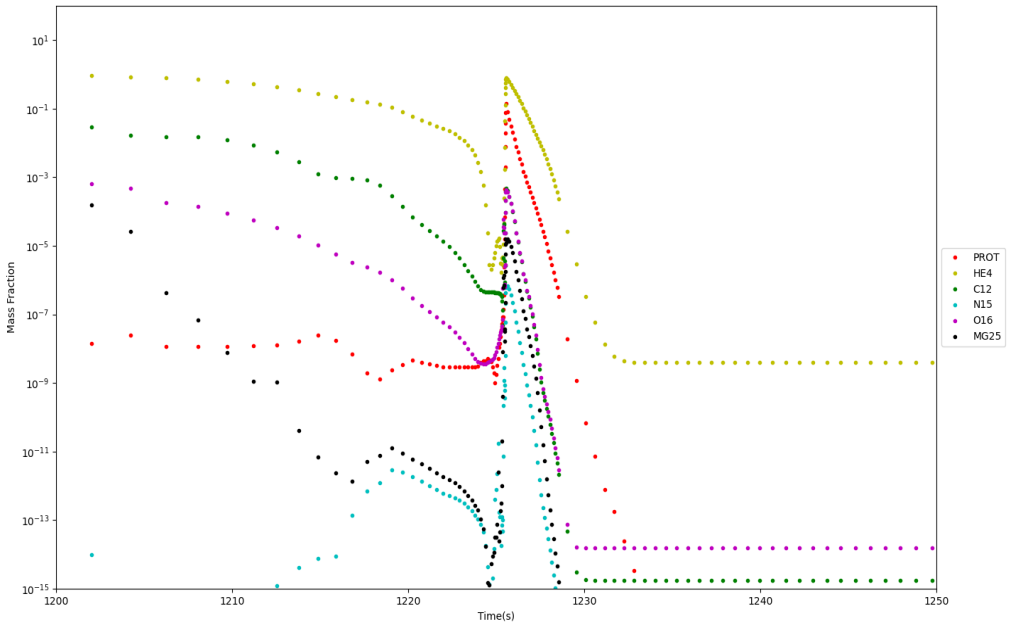

Figure 26: For the old reaction rate; the mass fraction over time for accretion rate of 128x10^{-5} solar mass per second and a minimum radius of 13.86km.

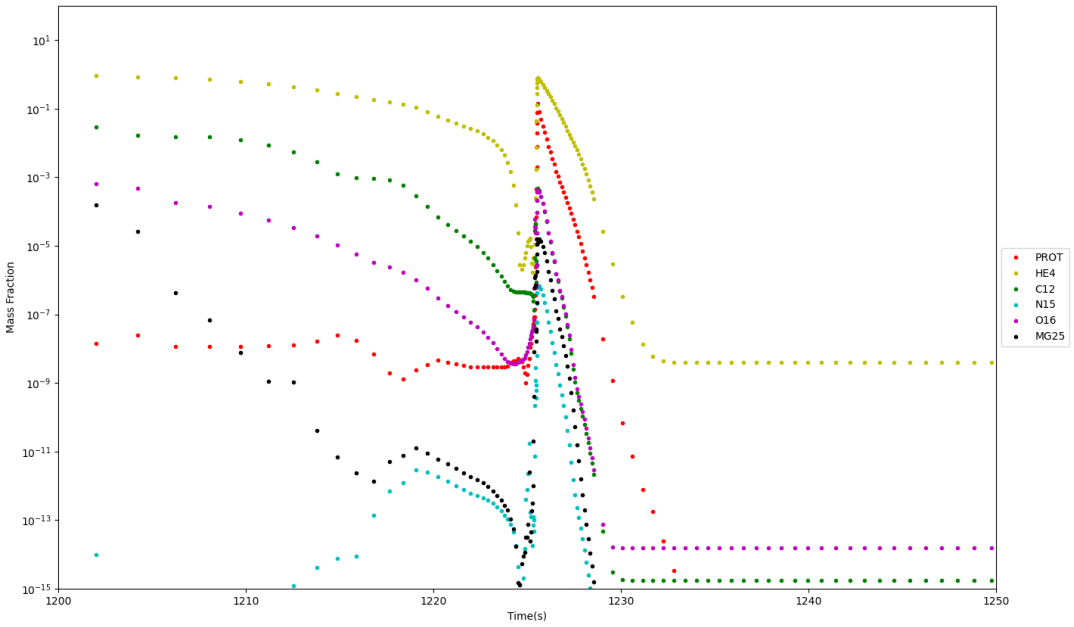

Figure 27: For the new reaction rate: mass fraction over time for accretion rate of 128x10^{-5} solar mass per second and a minimum radius of 13.86km.

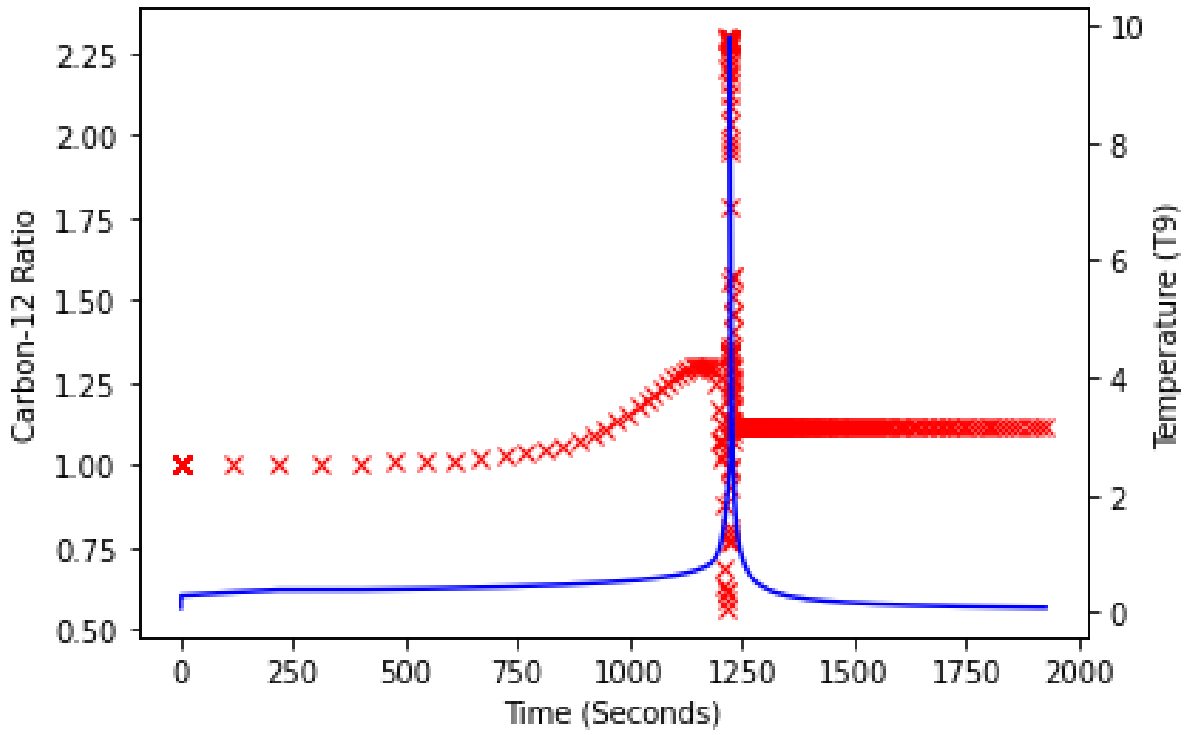

Figure 28: The ratio of the abundance of carbon-12 for the new and the old reaction rate and the temperature over time for 13.86km minimum radius and accretion rate of 128 solar mass per second.

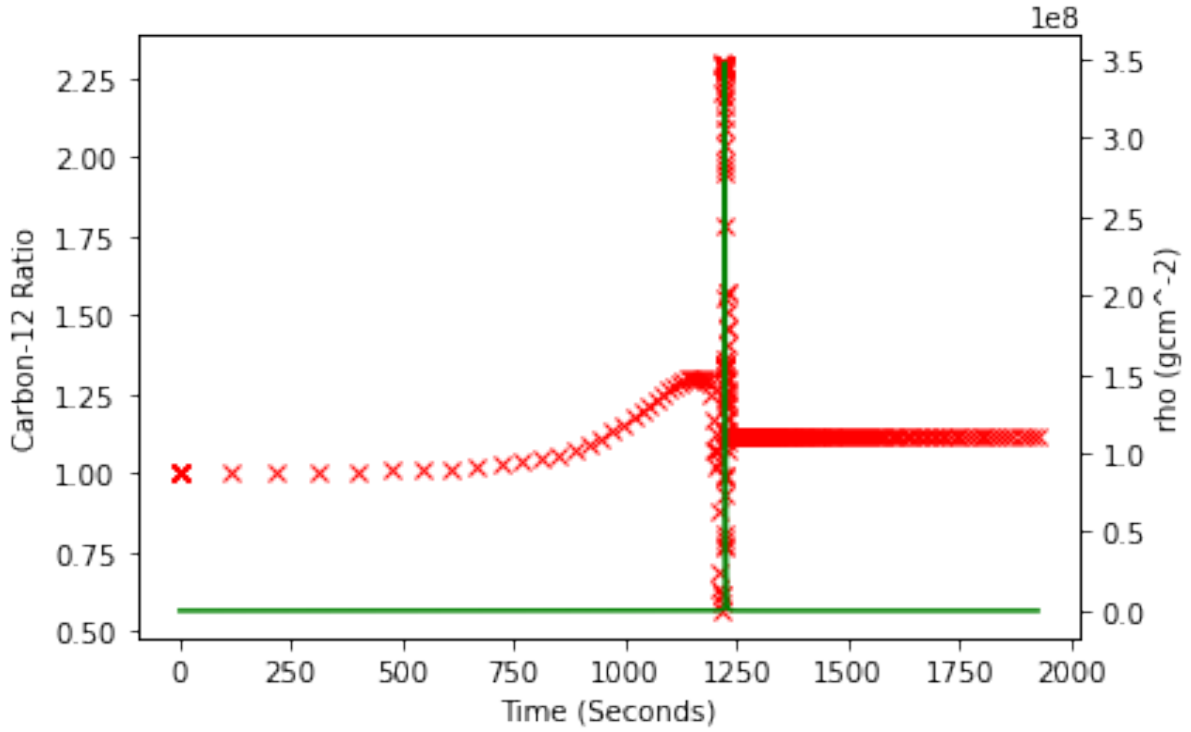

Figure 29: The ratio of the abundance of carbon-12 for the new and the old reaction rate and the density over time for 13.86km minimum radius and accretion rate of 128 solar mass per second.

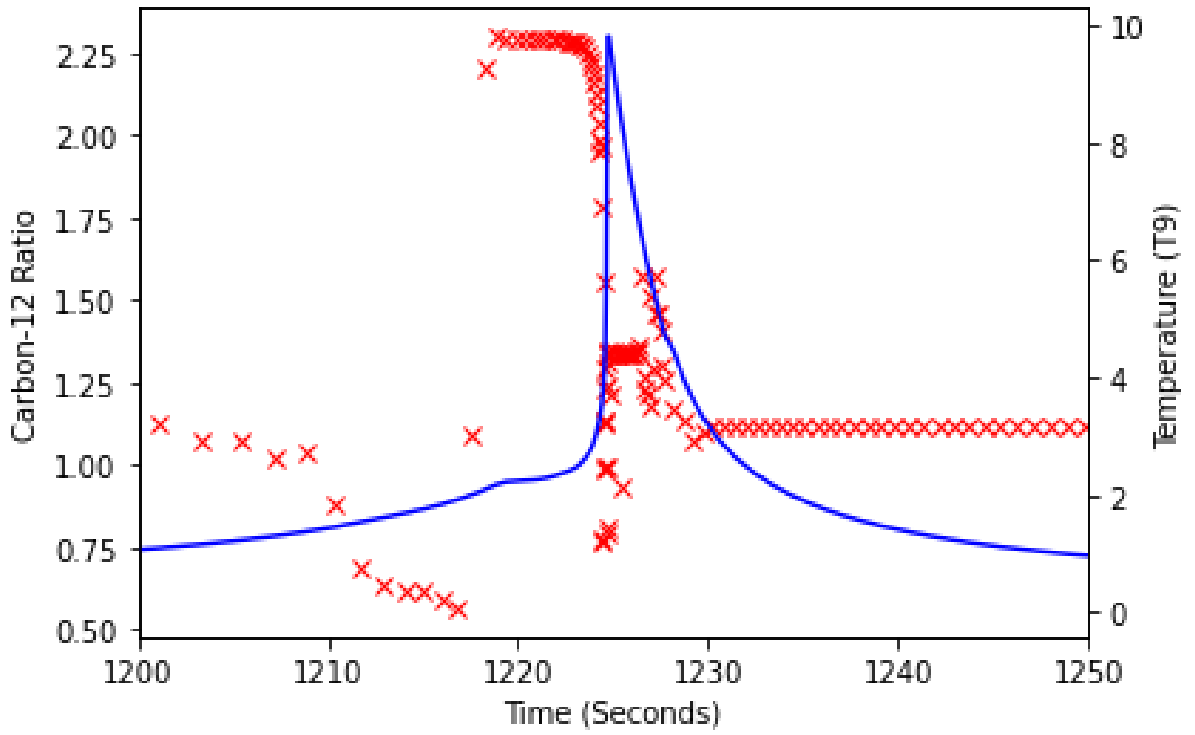

Figure 30: The ratio of the abundance of carbon-12 for the new and the old reaction rate and the temperature over time for 13.86km minimum radius and accretion rate of 256 solar mass per second.

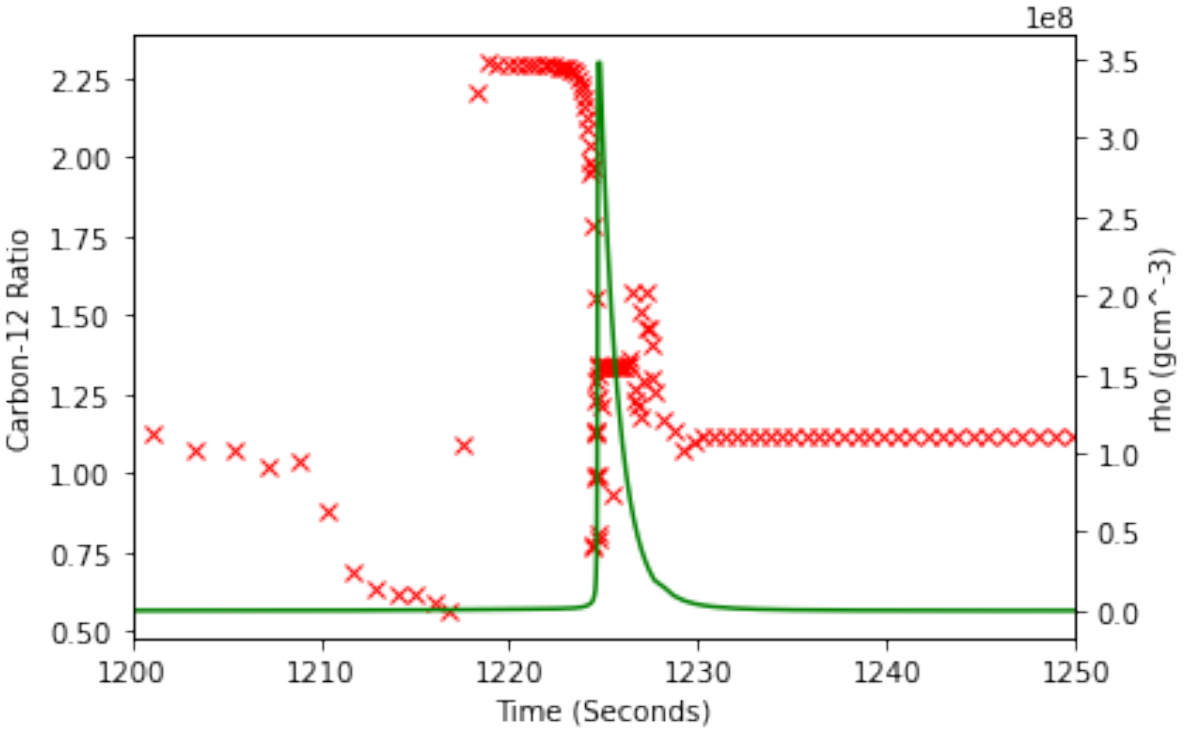

Figure 31: Carbon-12 ratio and density data for accretion rate 256x10^{-5} solar mass per second and minimum radius 13.86km

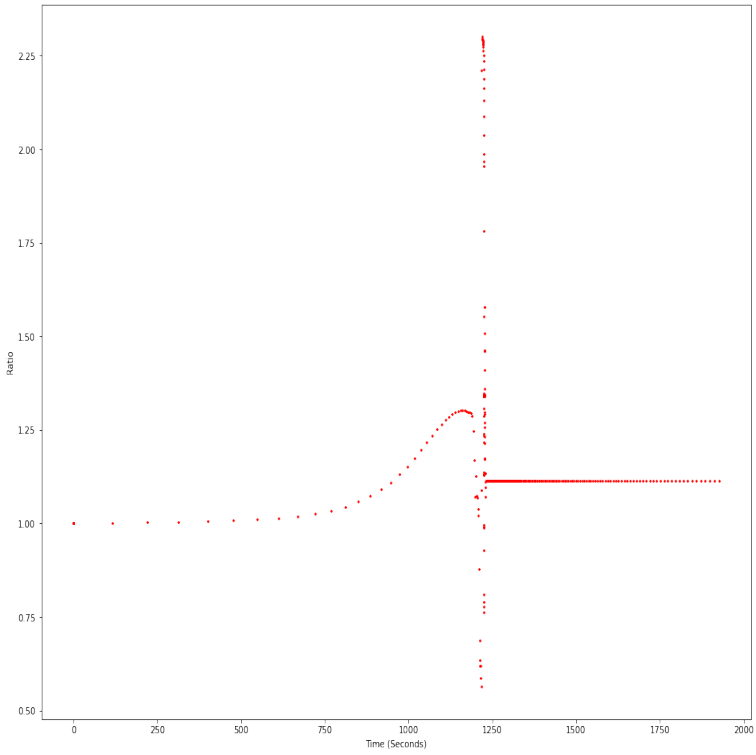

Figure 32: Carbon abundance ratio for accretion rate of 256x10^{-5} solar mass and minimum radius of 13.86km.

When the ratio of carbon-12 at each time step from the trajectories is calculated (adjusted rate abundance/old rate abundance) and plotted in figures 24-32 it is clear that there is a significant change in the ratio of carbon. It follows that as the temperature and more importantly density spike and increase the abundance of carbon-12 increases drastically. It's hard to say exactly what is happening however I would suggest that as the temperature and density rise the temperature reaches the threshold for fusion and then hits the temperature region where the triple alpha process tends to occur most which is just over 1 gigakelvin. The higher reaction rate results in higher carbon-12 abundance. The temperature and pressure rapidly spike, in the cases of figure 30 and 31 this results in initially greater fusion but then actually the breakdown of some heavier isotopes which leads to the brief spike in carbon-12 abundance, as the temperature and density then decrease within the trajectories the triple alpha process takes back over as the dominant force behind the formation of carbon-12, so the abundance spikes back up. The dip immediately after the spike can be explained by the higher temperature and density and the breakdown of heavier isotopes leading to an abundance of lighter elements to fuse with to form heavier isotopes again. This increase in abundance in the adjusted reaction rate models occurs in every simulation I have run. Although for a variety of accretion rates where the temperature spikes and density spike and stays elevated for longer (figures 30 and 31) it occurs slightly ahead of the extreme spikes (which are to be expected as the process is known as "explosive nucleosynthesis") and it appears clear looking at figure 30 in particular that the extreme temperature present at approximately 1205 seconds, in-fact causes the amount of carbon to briefly plummet before surging as the temperature and pressure increase considerably. This is due to either the breaking up of alpha particles before they can fuse or the fusing of carbon-12 to form heavier isotopes. Following this dip carbon production then increases considerably . Figure 32 shows the increase in Carbon-12 abundance throughout the simulation quite well, which is why I have included that plot, just showing the ratio of carbon-12 abundance between the two reaction rates. It is clear this way that even at the lower temperatures there is significantly more Carbon-12 present than when the new reaction rate has been used in the simulations than when the old reaction rate was used. The same pattern can be seen in the smaller 11km minimum radius trajectories too as well as the slower accretion rates I tested.

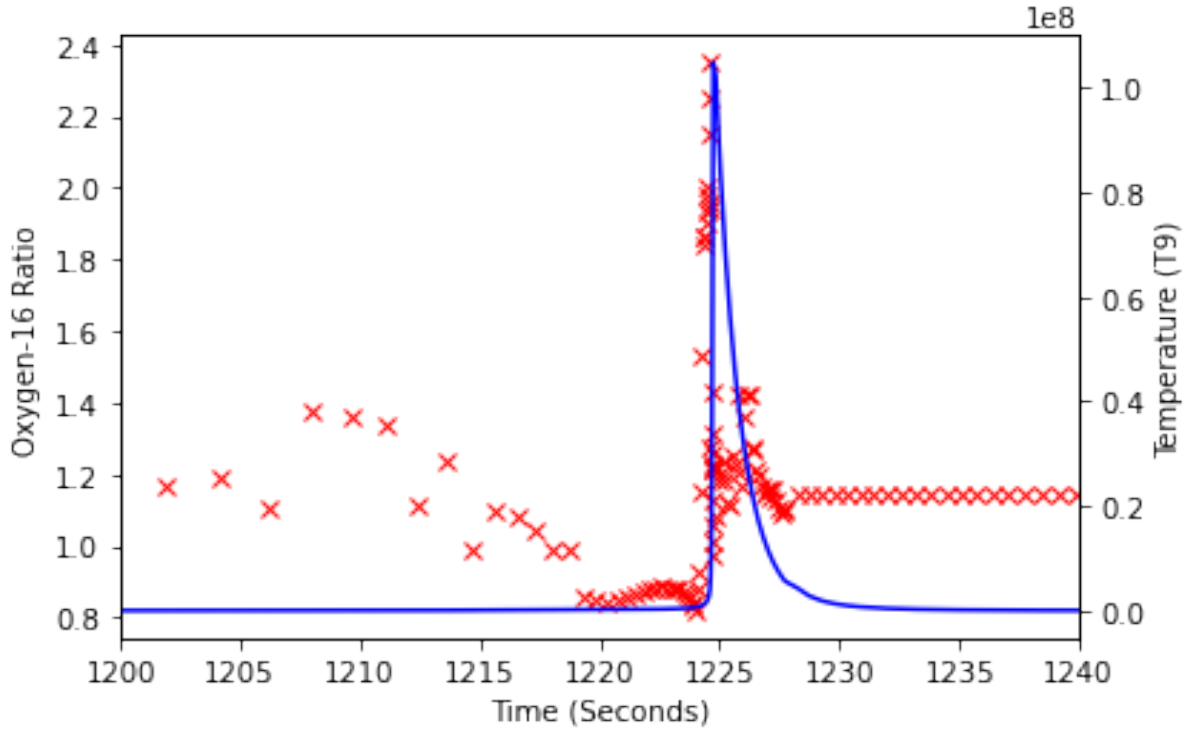

Figure 33: Oxygen ratio and temperature data plotted over time for accretion rate 64x10^{-5} solar mass and minimum radius of 11.12km.

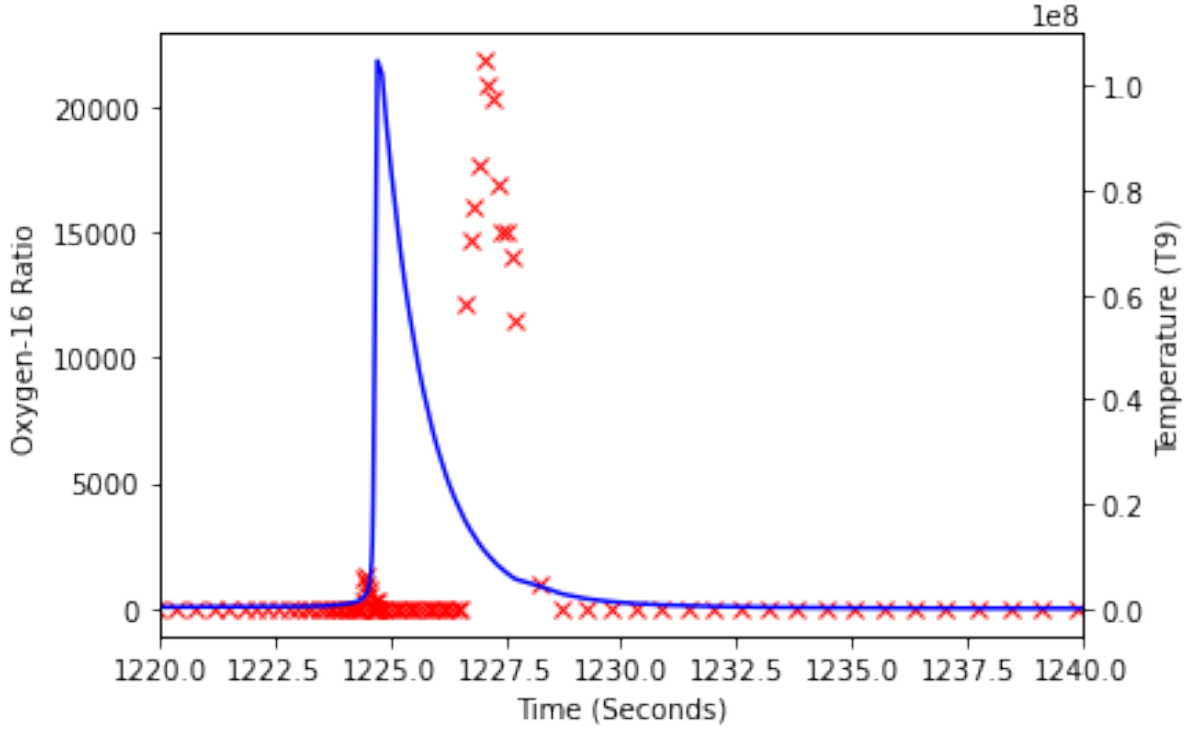

Figure 34: Oxygen ratio and temperature data plotted over time for accretion rate 64x10^{-5} solar mass and minimum radius of 13.86km.

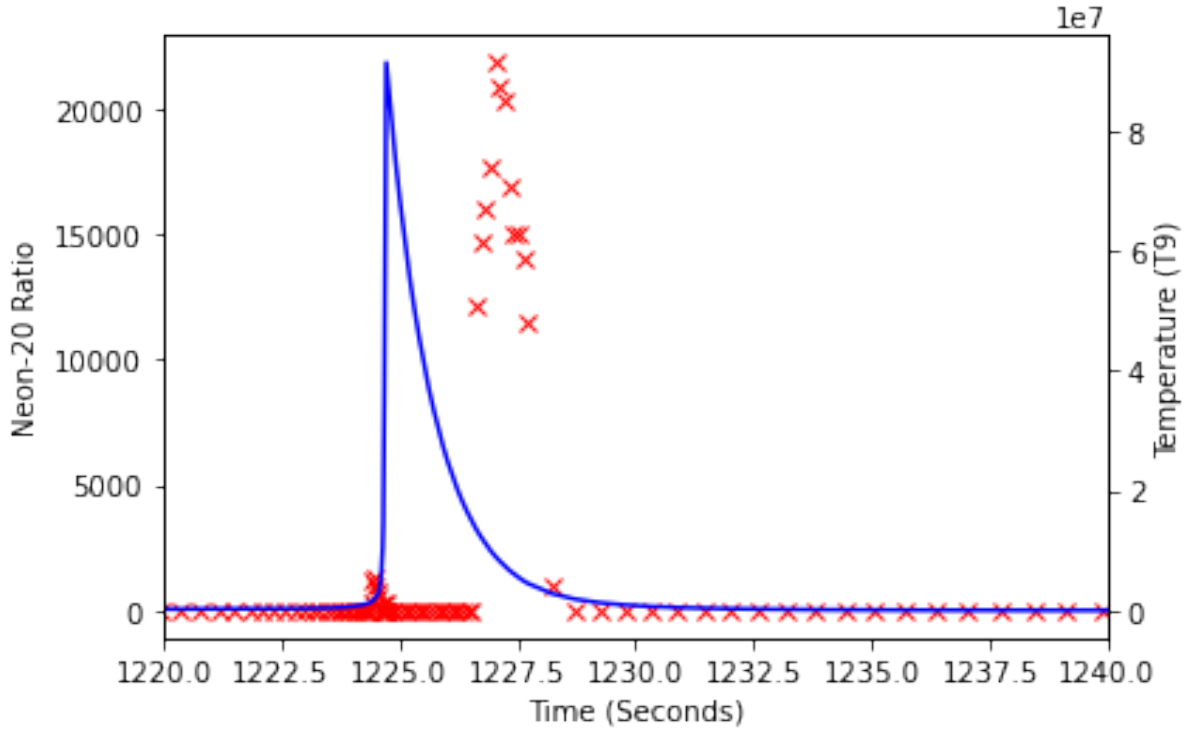

Figure 35: Neon ratio and temperature data plotted over time for accretion rate 64x10^{-5} solar mass and minimum radius of 13.86km.

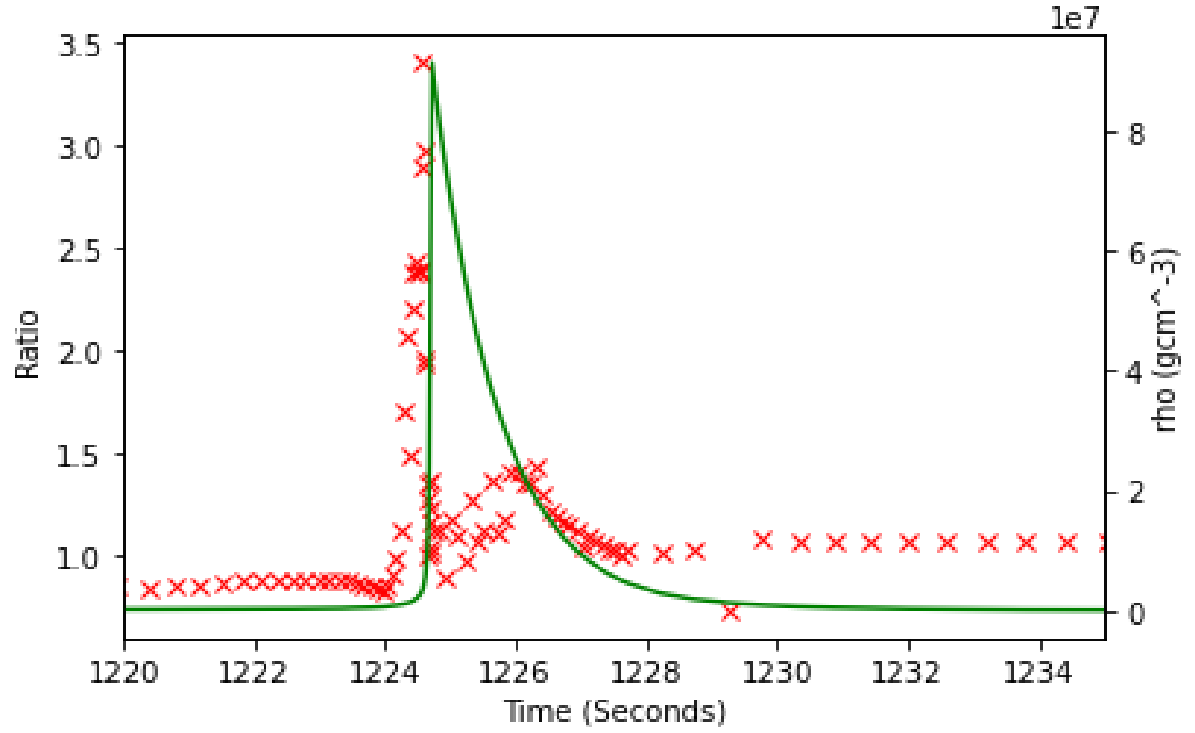

Figure 36: Neon-20 ratio and temperature data plotted over time for accretion rate 64x10^{-5} solar mass and minimum radius of 13.86km.

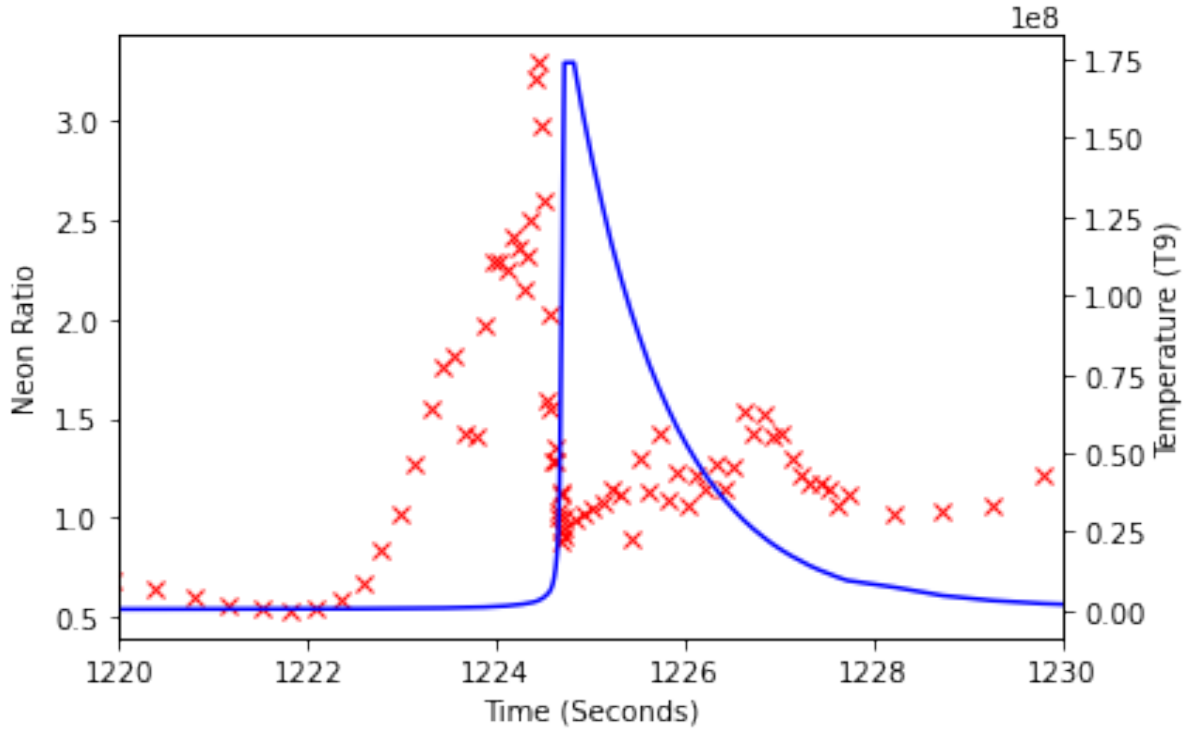

Figure 37: Neon-20 ratio and temperature data plotted over time for accretion rate 128x10^{-5} solar mass and minimum radius of 13.86km.

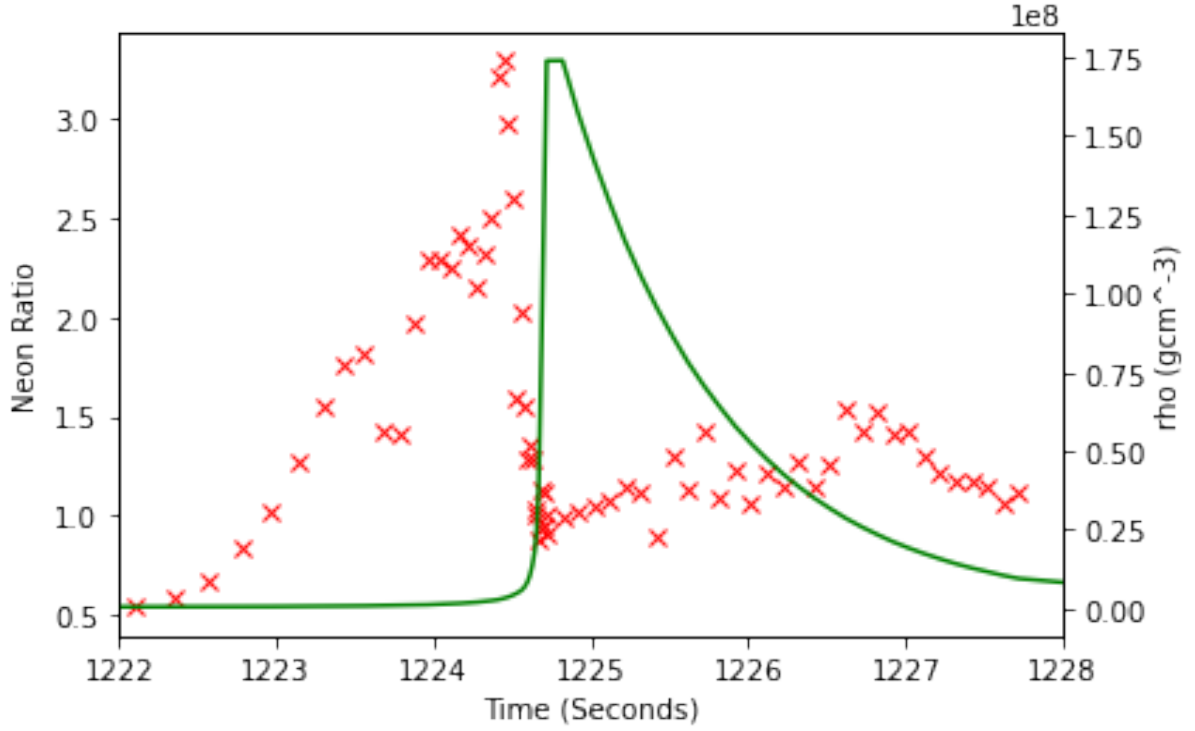

Figure 38: Neon-20 ratio and temperature data plotted over time for accretion rate 128x10^{-5} solar mass and minimum radius of 13.86km.

Figures 33 and 34 show the ratio of the abundance of oxygen between the original and adjusted reaction rate and figures 35 and 36 show the same for neon-20. These figures are for the same 2 minimum radii (13.86km and 11.12 km) and the same accretion rate of 64x10^{-5} solar mass per second. As you can see clearly there is an increase throughout the simulations in the abundance of oxygen, as there was with carbon. Both see high peaks in abundance as temperature and density spike and initially cause reactions to increase and then plummet (as temperatures get too high and start to cause isotopes to breakdown). carbon-12 and oxygen abundance still remains significantly higher in the simulations using the adjusted reaction rate than those using the old reaction rate. The same is true of neon-20, as the plots in figures 35-38 show although the difference was slightly less pronounced but still significant.

8 Conclusions

In conclusion, the data presented in the previous section clearly suggests that a reaction rate for carbon-12, 30 percent higher than the previous accepted rate, does have a significant effect on the abundance of carbon-12 in nucleosynthesis models. This is the first time this has been investigated in this astrophysical environment and it suggests that nucleosynthesis models involving the triple alpha rate are likely to be significantly impacted by the new accepted value for Γ_{rad}. In addition to this, I have also provided plots that show that this, causes changes to the abundances of various heavier elements such as oxygen and neon to further demonstrate how noticeable the impact an increased reaction rate could have on our understanding of nucleosynthesis and abundance of various isotopes. It seems likely from my graphs that the abundance of isotopes like oxygen-16 likely scales proportionally to the new carbon-12 resonant reaction rate. This proportional scaling should mean the carbon:oxygen ratio is unaffected, as an increased abundance of Carbon does appear to simply result in a similar increase in the abundance of Oxygen-16. I will include additional graphs for the trajectories mentioned in my results section that further demonstrate the effect of the reaction rate in my appendix.

The scope of my investigation into this may have been, limited; to investigating how a change in the radiative width would effect the reaction rate of carbon-12, and how that might have impact nucleosynthesis models. I believe that I have successfully demonstrated that in the astrophysical environment: a common envelope binary for a helium-burning late stage red dwarf donor star with a neutron star secondary star. On the neutron star the higher resonant reaction pathway rate has a significant impact upon the abundance of carbon-12 and as such the abundance of other elements that rely on the formation of carbon-12 as a step in the nucleosynthesis of those heavier isotopes.

Given the opportunity, were I redoing this project from scratch I think I would ideally have liked to try some rates for neutron stars with different solar masses rather than just for the 2.0 solar mass star I used. I would also perhaps have tried to run some hydrodynamic simulations, however these are complex to set up and due to their complexity they require alot more computational power availability and time. Instead I have used trajectories that originate from hydrodynamic simulations already run by Chris Fryer and provided to me by Alexander Hall-Smith.

These results suggest that there is plenty of evidence based on my results for further investigation. The direction this takes would be up to those doing the work, but I would suggest that a place to start might be recalculating its contribution to the overall combined reaction that incorporates resonant and non-resonant reaction pathways. Implementing that in NuGrid and being able to more accurately access the effect it has on models and perhaps with greater scope than just focusing on the abundance of carbon-12 but perhaps how this effects the abundance of a range of much heavier elements. An investigation to see how it might effect nucleosynthesis models in other scenarios would also be a valuable direction for future work to go in. Regardless, the impact of these results is clear in my view that current models are failing to take into account this increased rate of Carbon-12 formation and this has potentially impacts the whole nucleosynthesis model as it should have a knock on effect on the rate at which

greater mass elements/isotopes are formed.

Further research should be done into if the carbon:oxygen ratio is impacted by these results although it certainly appears that it isn't but it should definitely be checked that, that is the case as if it in-fact does it could have some profound impacts on our understanding on the isotopic makeup of the universe and could imply that the conditions that enable life, like us to exist may be broader than they are currently believed to be. It is also worth doing further studies to establish how medium mass elements abundances is effected and how that might impact models for nucleosynthesis of other much higher mass isotopes.

9 Appendix A: Reaction Rate Code

```python
import math
import numpy as np
import csv
```

```python
import matplotlib
matplotlib.use('TkAgg')
import matplotlib.pyplot as plt
```

```python
NA = 6.0221409E23 #Avagadros constant in particles per mole ^-1
K_B = 8.617E-5 #eV.K^-1
hbar = 6.582E-16 ##ev
pi = math.pi
Q = 379379.5349 #eV
gamma_rad = 3.896E-3         #    new radiative width from the 2020 paper.
M = 3725.976E6 #ev/c^2
f = (gamma_rad/hbar)
i = 1
T = 0
r = 0
c = 2.99E10 #cm/s
reaction_rate =[]
temperature =[]
rate= []
```

Figure 39: Reaction Rate Python Code Part-1

```
i=1
while i<=200:

    T = i/100
    T9 = T *10**9
    logT = math.log10(T9)
    temperature.append(T9)

    a = (3**(3/2)) * (6*(NA**2)) ##3^(3/2) *6

    b = 2*pi*((hbar**2)*(c**2)) ##2pi*hbar^2*c^2


    z = (M*K_B*T9)  ## 4M*KB*T9

    d = (-Q/(K_B*T9))  ##(-Q/(KB*T9))
    ##print('d =',d)
    x = (a *(((b/z)**3)*f)*math.exp(d)) ## (3^(3/2) * 6) * [(2pi * hbar^2)/(M * KB * T)] * (gamma_rad/hbar) e ^(-Q/KB*T)
    print('i =',i)
    print('log10(T) =',logT)
    print('x =', x)

    r = math.log10(x)
    print('r =',r)
    rate.append(x)
    reaction_rate.append(r)

    i= i+1
```

Figure 40: Python Code for reaction rate part-2

10 Appendix B: Additional Plots

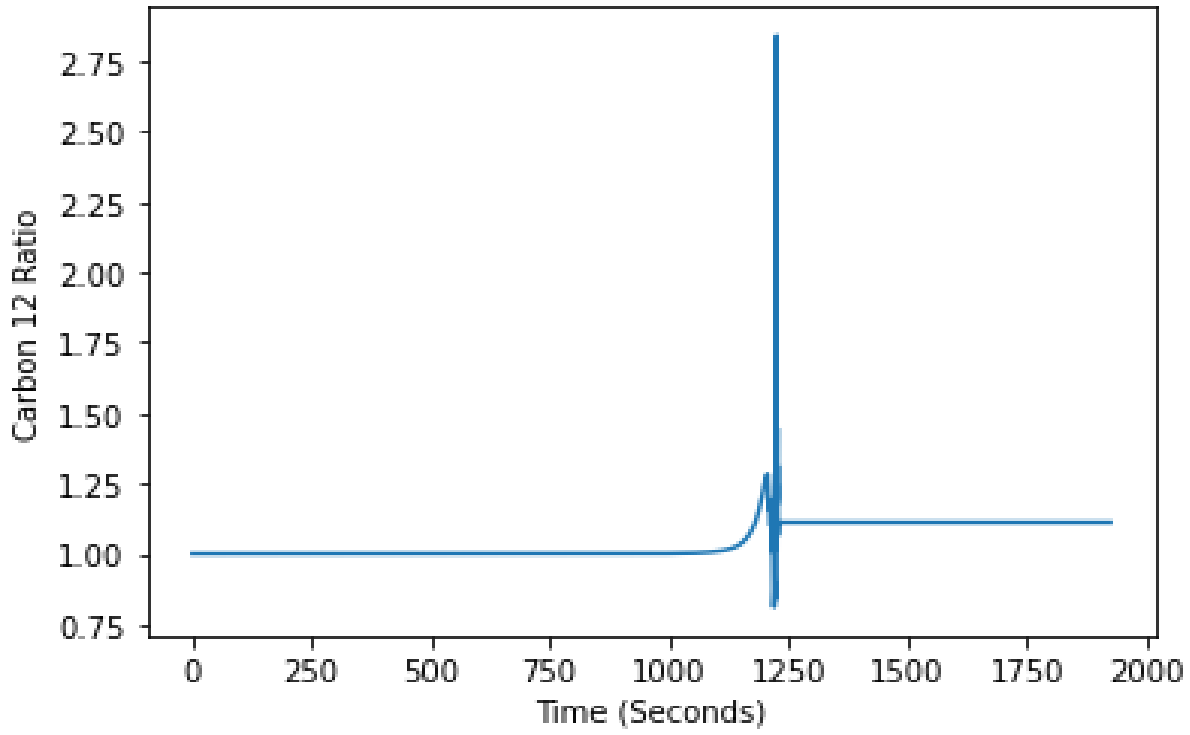

Figure 41: Carbon-12 ratio data plotted over time for accretion rate 64x10^{-5} solar mass and minimum radius of 13.86km.

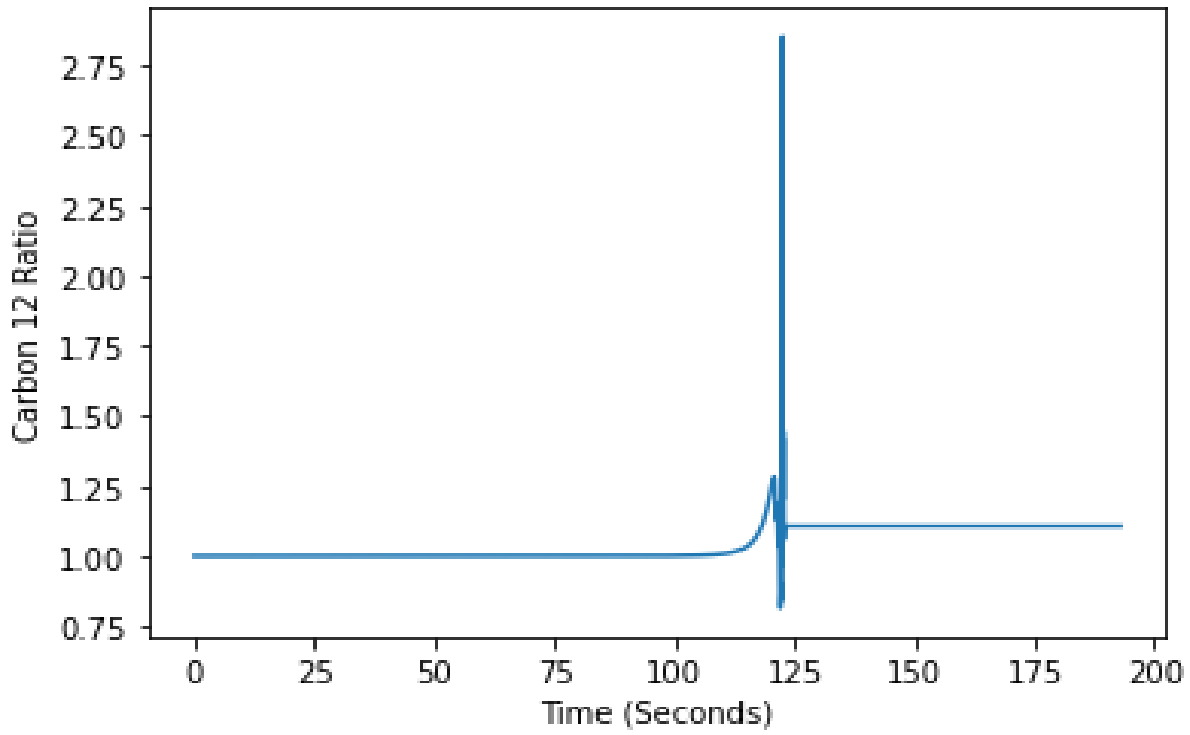

Figure 42: Carbon-12 ratio and temperature data plotted over time for accretion rate 64x10^{-5} solar mass and minimum radius of 11.12km.

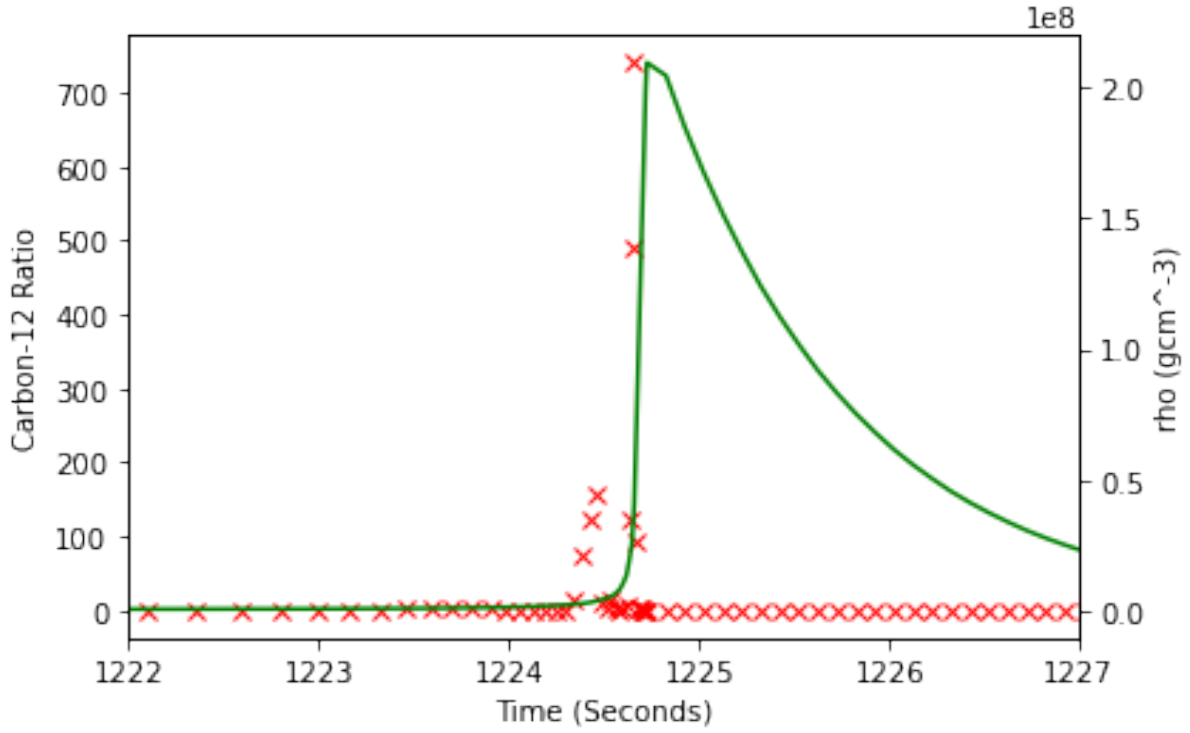

Figure 43: Carbon-12 ratio and density data plotted over time for accretion rate 128x10^{-5} solar mass and minimum radius of 11.12km.

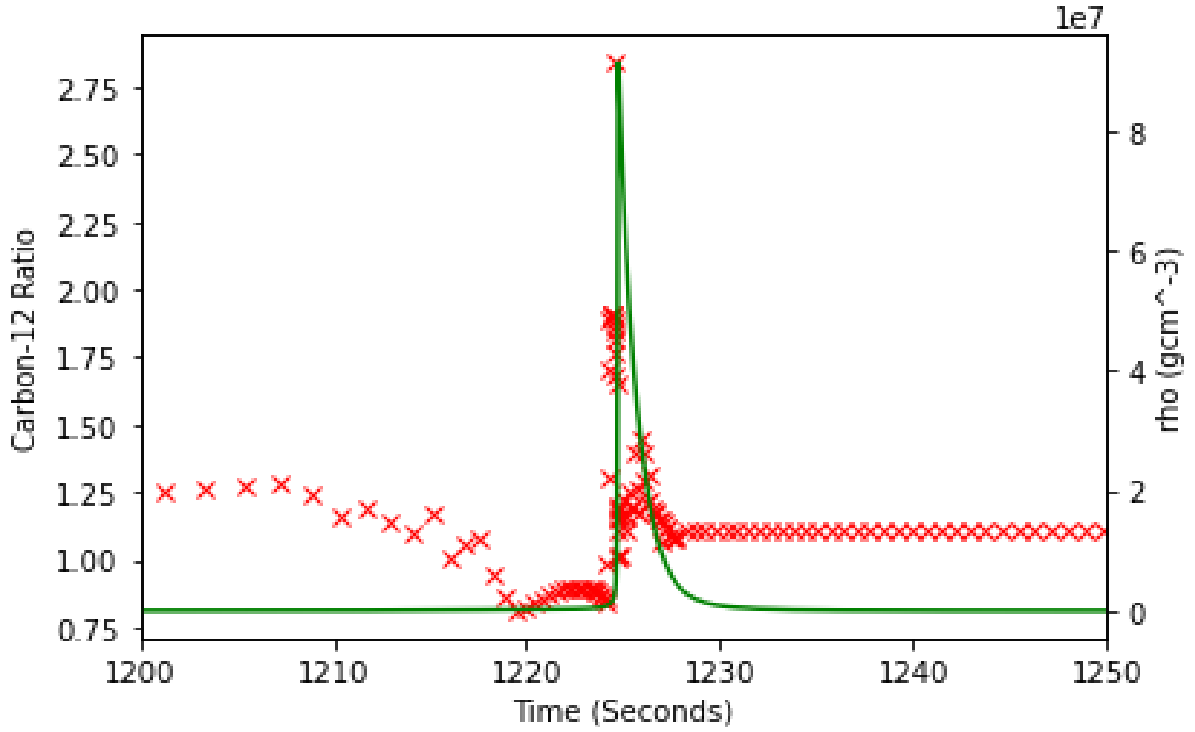

Figure 44: Carbon-12 ratio and density data plotted over time for accretion rate 64x10^{-5} solar mass and minimum radius of 13.86km.

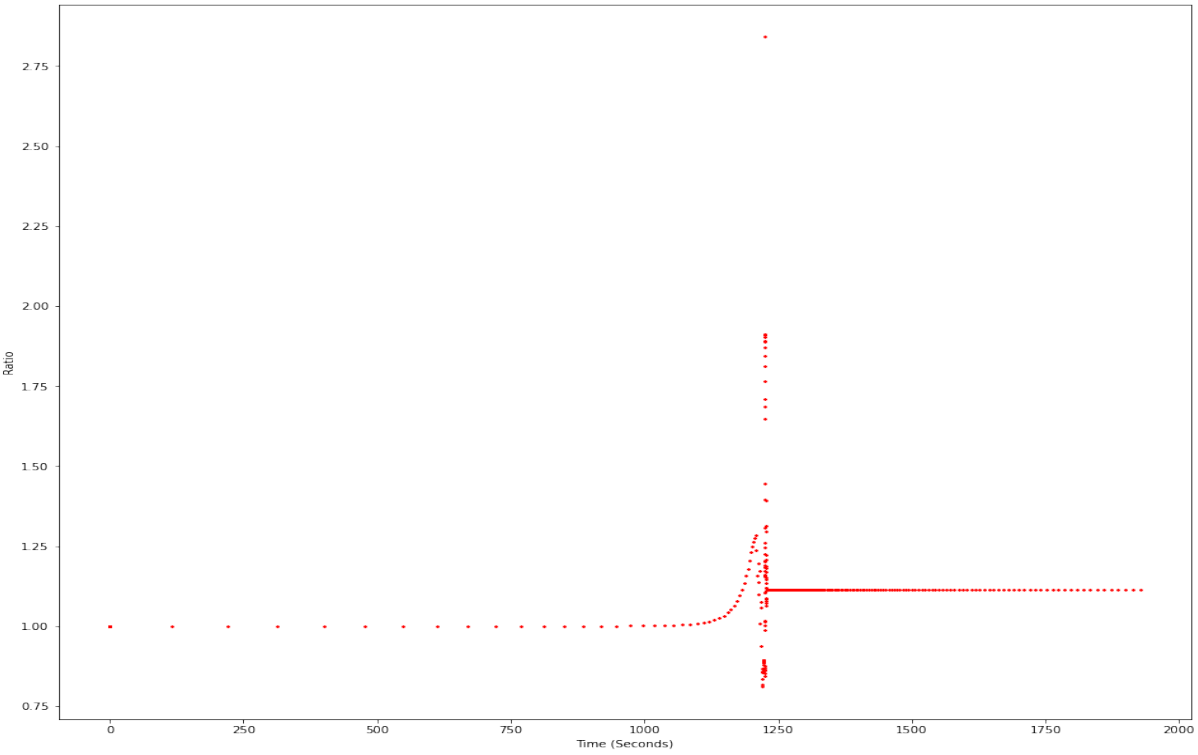

Figure 45: Carbon-12 ratio and temperature data plotted over time for accretion rate 64x10^{-5} solar mass and minimum radius of 13.86km.

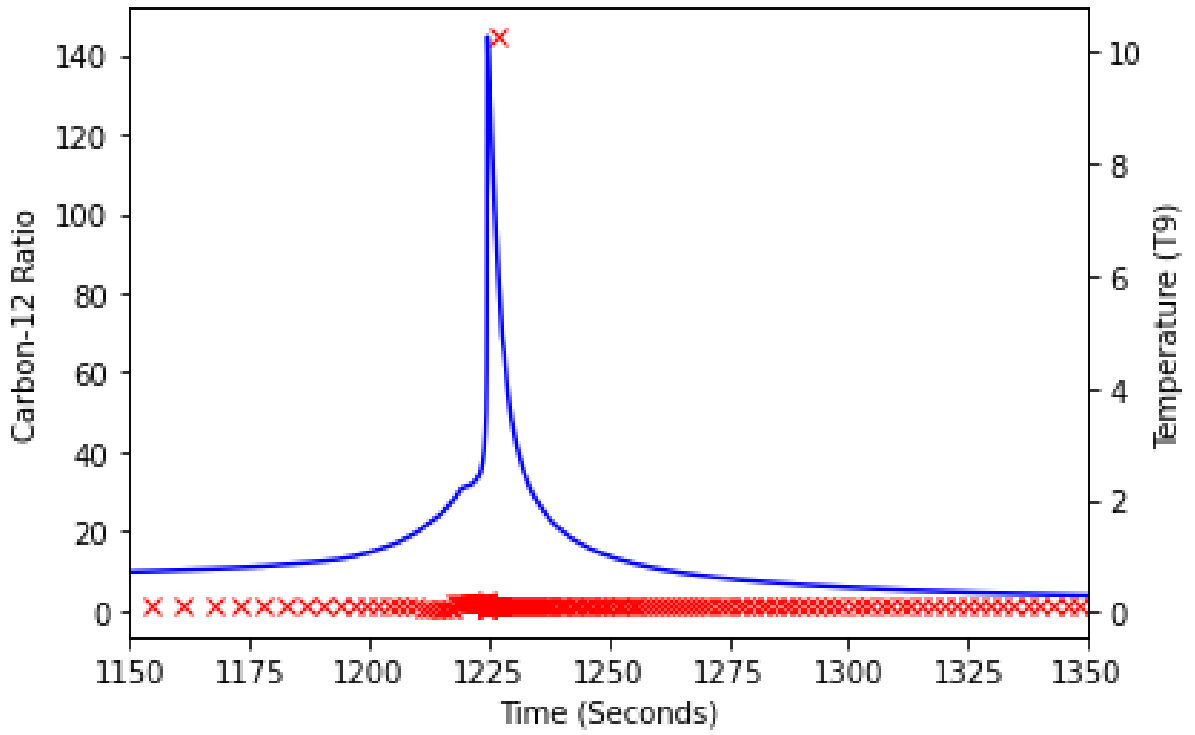

Figure 46: Neon-20 ratio and temperature data plotted over time for accretion rate 128x10^{-5} solar mass and minimum radius of 13.86km.

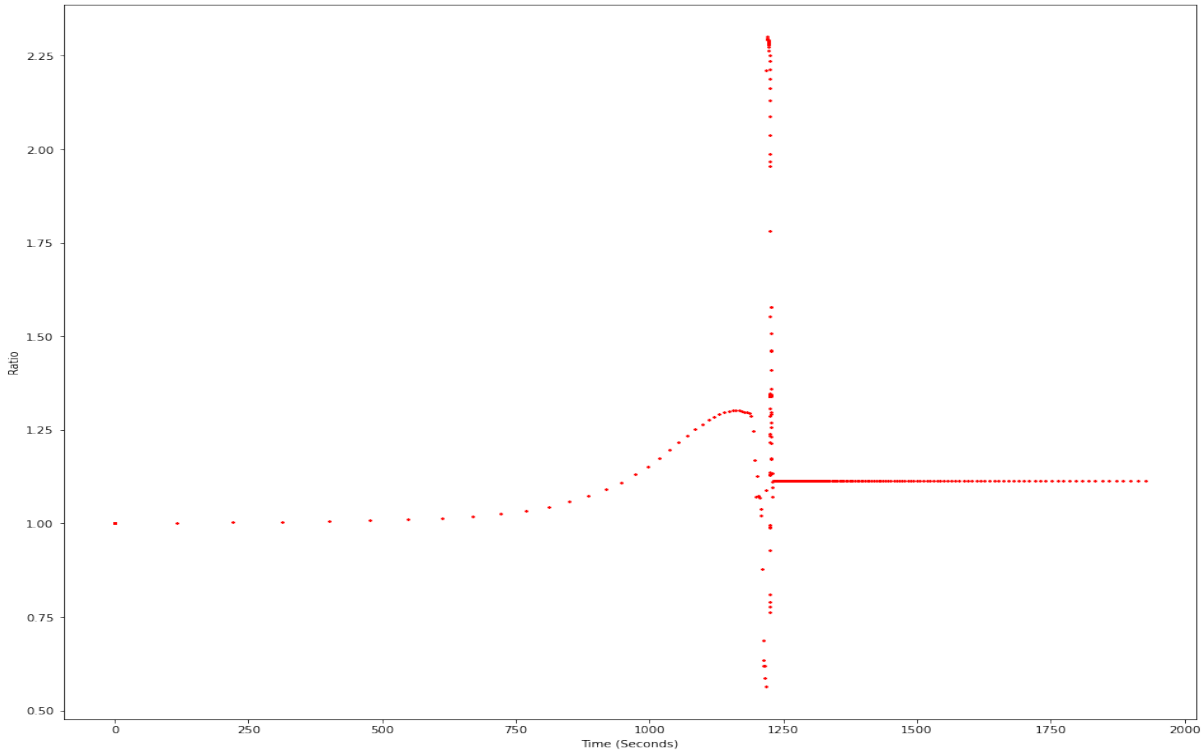

Figure 47: Carbon-12 ratio and temperature data plotted over time for accretion rate 256x10^{-5} solar mass and minimum radius of 13.86km.

Figure 48: Carbon-12 ratio and data plotted over time for accretion rate 256x10^{-5} solar mass and minimum radius of 11.12km.

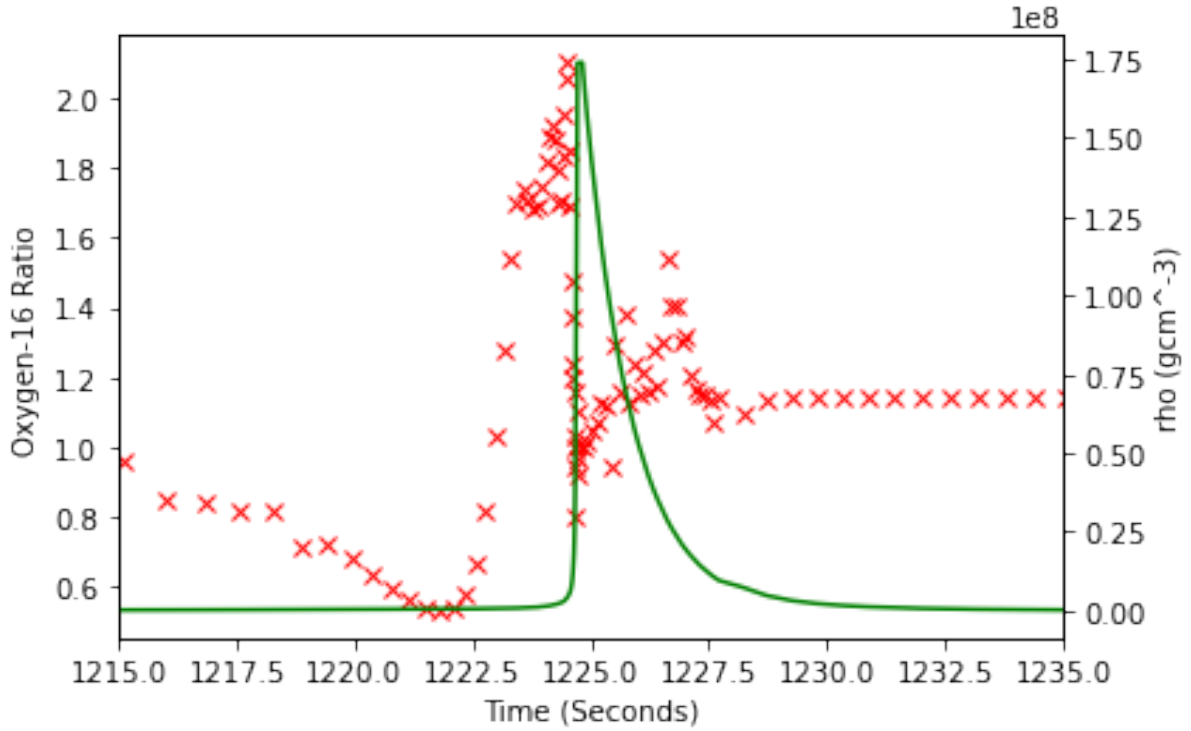

Figure 49: Oxygen-16 ratio and density data plotted over time for accretion rate 128x10^{-5} solar mass and minimum radius of 13.86km.

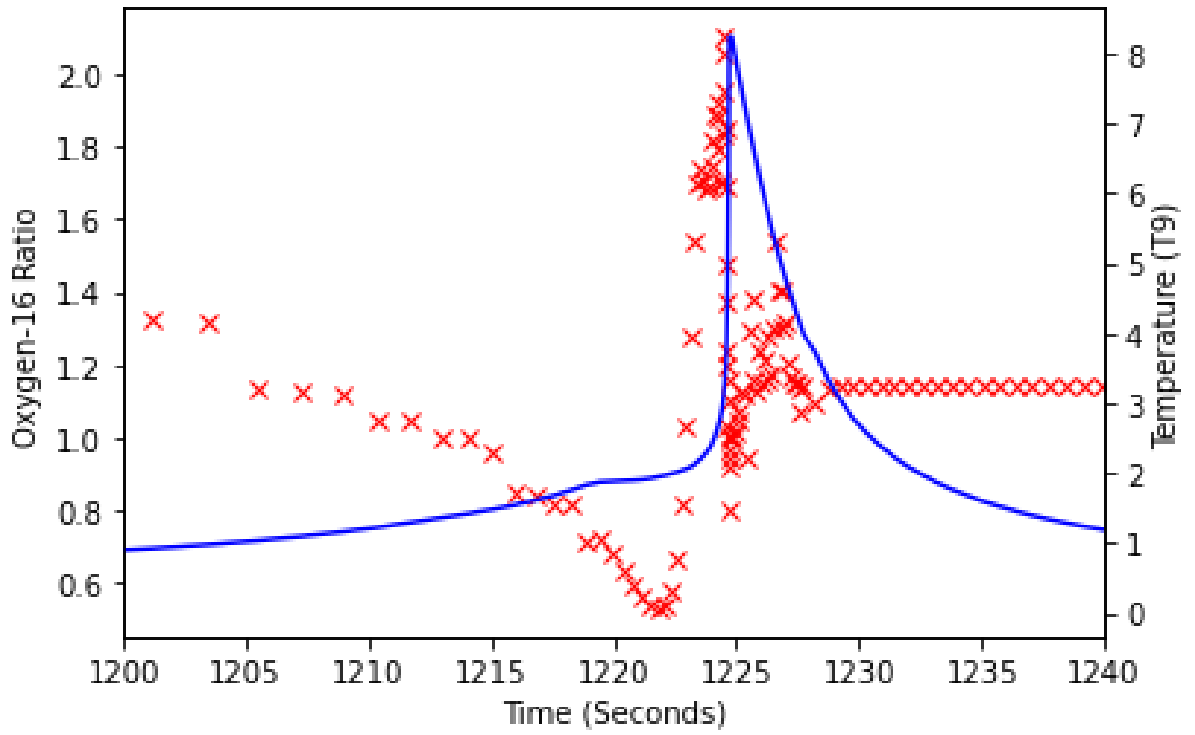

Figure 50: Oxygen-16 ratio and temperature data plotted over time for accretion rate 128x10^{-5} solar mass and minimum radius of 13.86km.

Figure 51: Carbon-12 ratio and temperature data plotted over time for accretion rate 256x10^{-5} solar mass and minimum radius of 11.12km.

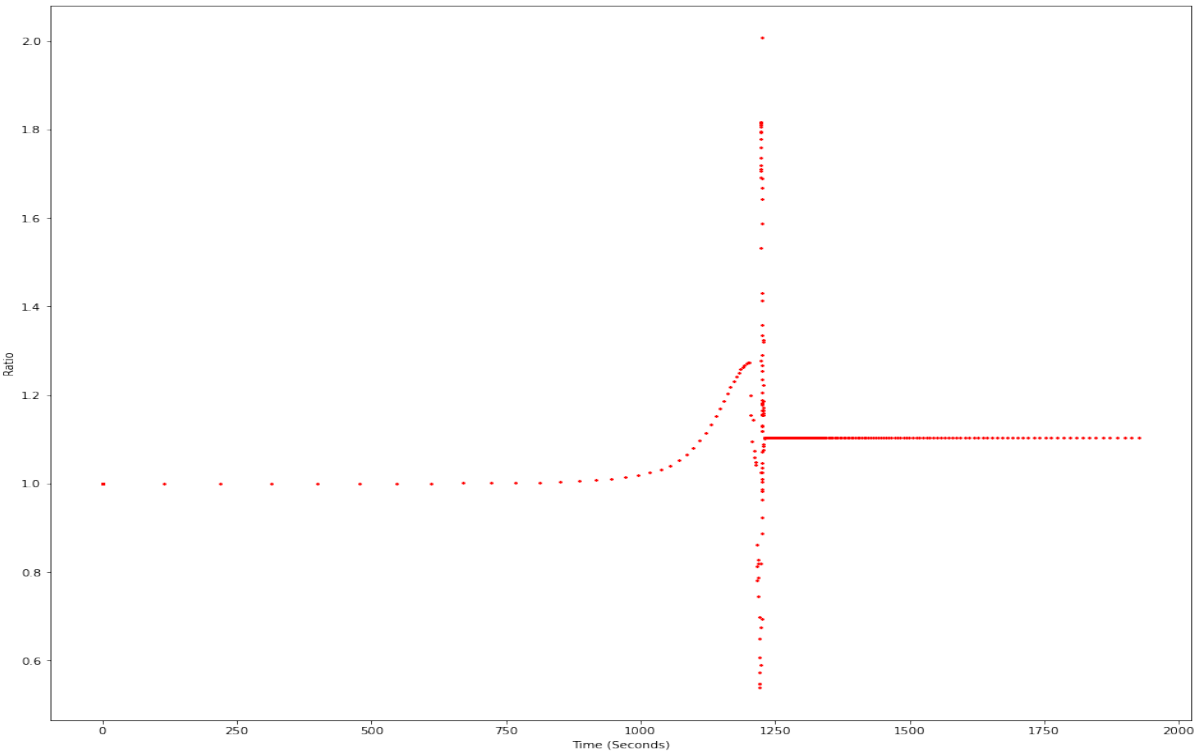

Figure 52: Carbon-12 ratio data plotted over time for accretion rate 128x10^{-5} solar mass and minimum radius of 13.86km.

References

[1] T. Kibédi, B. Alshahrani, A. E. Stuchbery, A. C. Larsen, A. Görgen, S. Siem, M. Guttormsen, F. Giacoppo, A. I. Morales, E. Sahin, G. M. Tveten, F. L. B. Garrote, L. C. Campo, T. K. Eriksen, M. Klintefjord, S. Maharramova, H.-T. Nyhus, T. G. Tornyi, T. Renstrøm, and W. Paulsen, "Radiative width of the hoyle state from γ-Ray spectroscopy," *Phys. Rev. Lett.*, vol. 125, p. 182701, Oct. 2020.

[2] T. Montmerle and S. Ekström, "Hertzsprung-Russell diagram," in *Encyclopedia of Astrobiology*, pp. 1099–1105, Berlin, Heidelberg: Springer Berlin Heidelberg, 2015.

[3] "Superfluidity." https://www.southampton.ac.uk/maths/research/projects/superfluidity.page. Accessed: 2023-8-1.

[4] "Roche-lobe." https://astronomy.swin.edu.au/cosmos/r/roche-lobe. Accessed: 2023-8-6.

[5] "Roche-lobe." https://astronomy.swin.edu.au/cosmos/r/roche-lobe. Accessed: 2023-8-6.

[6] M. Freer and H. O. U. Fynbo, "The hoyle state in 12C," *Prog. Part. Nucl. Phys.*, vol. 78, pp. 1–23, Sept. 2014.

[7] G. R. Caughlan and W. A. Fowler, "Thermonuclear reaction rates V," *At. Data Nucl. Data Tables*, vol. 40, pp. 283–334, Nov. 1988.

[8] H. O. U. Fynbo, C. A. A. Diget, U. C. Bergmann, M. J. G. Borge, J. Cederkäll, P. Dendooven, L. M. Fraile, S. Franchoo, V. N. Fedosseev, B. R. Fulton, W. Huang, J. Huikari, H. B. Jeppesen, A. S. Jokinen, P. Jones, B. Jonson, U. Köster, K. Langanke, M. Meister, T. Nilsson, G. Nyman, Y. Prezado, K. Riisager, S. Rinta-Antila, O. Tengblad, M. Turrion, Y. Wang, L. Weissman, K. Wilhelmsen, J. Aystö, and ISOLDE Collaboration, "Revised rates for the stellar triple-alpha process from measurement of 12C nuclear resonances," *Nature*, vol. 433, pp. 136–139, Jan. 2005.

[9] M. Pignatari and F. Herwig, "The NuGrid research platform: A comprehensive simulation approach for nuclear astrophysics," *Nuclear Physics News*, vol. 22, pp. 18–23, Oct. 2012.

[10] M. Pignatari and F. Herwig, "The NuGrid research platform: A comprehensive simulation approach for nuclear astrophysics," *Nuclear Physics News*, vol. 22, pp. 18–23, Oct. 2012.

[11] "Composition of the sun." http://hyperphysics.phy-astr.gsu.edu/hbase/Tables/suncomp.html. Accessed: 2024-1-5.

[12] M. Sandora, V. Airapetian, L. Barnes, G. F. Lewis, and I. Pérez-Rodríguez, "Multiverse predictions for habitability: Element abundances," *Universe*, vol. 8, p. 651, Dec. 2022.

[13] M. Freer and H. O. U. Fynbo, "The hoyle state in 12C," *Prog. Part. Nucl. Phys.*, vol. 78, pp. 1–23, Sept. 2014.

[14] "NASA - one weird type of star acts like another,"

[15] "Binary star systems: Classification and evolution." https://www.space.com/22509-binary-stars.html, Jan. 2018. Accessed: 2023-6-7.

[16] "Binary star systems: Classification and evolution." https://www.space.com/22509-binary-stars.html, Jan. 2018. Accessed: 2023-6-7.

[17] "Binary star systems: Classification and evolution." https://www.space.com/22509-binary-stars.html, Jan. 2018. Accessed: 2023-6-7.

[18] E. Burns, "Neutron star mergers and how to study them," *Living Rev. Relativ.*, vol. 23, p. 4, Nov. 2020.

[19] I. Iben and M. Livio, "COMMON ENVELOPES IN BINARY STAR EVOLUTION," *PASP*, vol. 105, p. 1373, Dec. 1993.

[20] "Red giant stars." https://astronomy.swin.edu.au/cosmos/r/Red+giant+stars. Accessed: 2023-6-1.

[21] Y. Lim and J. W. Holt, "Neutron star radii, deformabilities, and moments of inertia from experimental and ab initio theory constraints on the 208pb neutron skin thickness," Apr. 2022.

[22] "Stars: Neutron stars, pulsars and magnetars." https://www.esa.int/Science$_{E}xploration/Space_{S}cience/Stars_{N}eutron_{s}tars_{p}ulsars_{a}nd_{m}agnetars.Acce$
$2023-6-1.$

[23] C. Thompson and R. C. Duncan, "The soft gamma repeaters as very strongly magnetized neutron stars - i. radiative mechanism for outbursts," *Mon. Not. R. Astron. Soc.*, vol. 275, pp. 255–300, July 1995.

[24] S. A. Olausen and V. M. Kaspi, "THE McGILL MAGNETAR CATALOG," *Astrophys. J. Suppl. Ser.*, vol. 212, p. 6, Apr. 2014.

[25] "ESA science & technology - equation of state for neutron stars." https://sci.esa.int/web/loft/-/49338-equation-of-state-for-neutron-stars. Accessed: 2023-7-12.

[26] Z. Arzoumanian, A. Brazier, S. Burke-Spolaor, S. Chamberlin, S. Chatterjee, B. Christy, J. M. Cordes, N. J. Cornish, F. Crawford, H. Thankful Cromartie, K. Crowter, M. E. DeCesar, P. B. Demorest, T. Dolch, J. A. Ellis, R. D. Ferdman, E. C. Ferrara, E. Fonseca, N. Garver-Daniels, P. A. Gentile, D. Halmrast, E. A. Huerta, F. A. Jenet, C. Jessup, G. Jones, M. L. Jones, D. L. Kaplan, M. T. Lam, T. J. W. Lazio, L. Levin, A. Lommen, D. R. Lorimer, J. Luo, R. S. Lynch, D. Madison, A. M. Matthews, M. A. McLaughlin, S. T. McWilliams, C. Mingarelli, C. Ng, D. J. Nice, T. T. Pennucci, S. M. Ransom, P. S. Ray, X. Siemens, J. Simon,

R. Spiewak, I. H. Stairs, D. R. Stinebring, K. Stovall, J. K. Swiggum, S. R. Taylor, M. Vallisneri, R. van Haasteren, S. J. Vigeland, W. Zhu, and The NANOGrav Collaboration, "The NANOGrav 11-year data set: High-precision timing of 45 millisecond pulsars," *ApJS*, vol. 235, p. 37, Apr. 2018.

[27] F. Hoyle and R. A. Lyttleton, "On the accretion of interstellar matter by stars," *Math. Proc. Cambridge Philos. Soc.*, vol. 36, pp. 325–330, July 1940.

[28] J. D. Keegans, *An Investigation into Nucleosynthesis in Common Envelope Neutron Star Systems*. PhD thesis, University of York, Jan. 2017.

[29] "High-Energy astrophysics, garret cotter, office 756 DWB, michaelmas 2012 lecture 7.pdf."

[30] "CODATA value: electron mass energy equivalent in MeV." https://physics.nist.gov/cgi-bin/cuu/Value?mec2mev. Accessed: 2023-8-12.

[31] W. Greiner and D. N. Poenaru, "Radioactivity," Jan. 2005.

[32] "Iron - element information, properties and uses." https://www.rsc.org/periodic-table/element/26/iron. Accessed: 2023-8-13.

[33] P. Dutta, "Radium-226." https://www.chemistrylearner.com/radium-226.html, Dec. 2018. Accessed: 2023-8-13.

[34] "Nuclear fusion." http://hyperphysics.phy-astr.gsu.edu/hbase/NucEne/fusion.html. Accessed: 2023-8-13.

[35] G. Towell, "Wave-particle duality: An overview." https://sciencing.com/wave-particle-duality-an-overview-13725853.html, Mar. 2020. Accessed: 2023-8-13.

[36] C. E. Rolfs and W. S. Rodney, *Cauldrons in the Cosmos: Nuclear Astrophysics*. University of Chicago Press, 1988.

[37] C. E. Rolfs and W. S. Rodney, *Cauldrons in the Cosmos: Nuclear Astrophysics*. University of Chicago Press, 1988.

[38] V. Singh, J. Lahiri, and D. N. Basu, "Theoretical exploration of s-factors for nuclear reactions of astrophysical importance," *Nucl. Phys. A*, vol. 987, pp. 260–273, July 2019.

[39] S. Jin, L. F. Roberts, S. M. Austin, and H. Schatz, "Enhanced triple-α reaction reduces proton-rich nucleosynthesis in supernovae," *Nature*, vol. 588, pp. 57–60, Dec. 2020.

[40] "Bose-Einstein condensation –." https://physicsworld.com/a/bose-einstein-condensation/, Mar. 1997. Accessed: 2023-8-7.

[41] M. Freer and H. O. U. Fynbo, "The hoyle state in 12C," *Prog. Part. Nucl. Phys.*, vol. 78, pp. 1–23, Sept. 2014.

[42] C. A. Diget, *Beta delayed particle emission: Probing the triple alpha continuum*. PhD thesis, Jan. 2006.

[43] H. Trac and U. Pen, "A primer on eulerian computational fluid dynamics for astrophysics," *PASP*, vol. 115, p. 303, Mar. 2003.

[44] "NuGrid collaboration." https://nugrid.github.io/. Accessed: 2023-12-22.

[45] C. L. Fryer, "Radiation hydrodynamics in astrophysics," in *Computational Methods in Transport*, pp. 1–14, Springer Berlin Heidelberg, 2006.

[46] R. C. (), "The JINA reaclib database." https://reaclib.jinaweb.org/. Accessed: 2023-12-22.